Rainbow River Vegetation, Filamentous Algae and Benthic Sediment Assessment

Prepared by the University of Florida for the Southwest Florida Water Management District

September 15, 2017

Robert T. Hensley, Nelson Anderson, Matthew J. Cohen, Larry V. Korhnak, and Chad R. Foster

Table of Contents

Executive Summary

Rainbow River is located in Marion County Florida, northeast of the city of Dunnellon. This spring fed river is formed by a multitude of spring vents which discharge ground water from the Floridan Aquifer System. The river flows in a generally southward direction for approximately 9.5 km (6 miles), where it joins the Withlacoochee River. Average historic flows have ranged between 28-13 m^3/s (640-297 million gallons/day). The average channel width is 55 m (~180 ft) while the average depth is 1.5 m (~5 ft). The headsprings are located within Rainbow Springs State Park. The entire length of the river itself is part of the Rainbow River Aquatic Preserve, and has been designated an Outstanding Florida Water. While this report will focus primarily on ecological aspects, it is important to keep in mind that Rainbow River also has significant socio-economic value. In addition to enhanced property values, resource-based recreational activities such as swimming, tubing, kayaking and SCUBA diving contribute substantially to the local economy.

Over the past decades, many spring-fed rivers in Florida have experienced a marked decline in native vascular submerged aquatic vegetation (SAV) and the proliferation of filamentous algal mats (Stevenson et al. 2004). While the traditional narrative has linked the proliferation of algae with nitrate (NO_3^-) enrichment from agricultural fertilizer runoff and wastewater effluent, remarkably little correlation between NO_3^- concentrations and rates of primary production (Odum 1957a, Canfield and Hoyer 1988, Duarte and Canfield 1990) or algal growth (Cowell and Botts 1994, Notestein et al. 2003) have been observed. Moreover, no correlation between NO_3^- concentrations and various measures of filamentous algal abundance has been observed, either within (Cowell and Botts 1994, Hoyer et al. 2004) or across (Stevenson et al. 2007, Heffernan et al. 2010) Florida's springs.

In Rainbow River, NO_3^- at the spring vent has risen from 0.08 mg/L historically (Odum 1957b) to over 2 mg/L at the time of this study. Concentrations of NO_3^- within the Rainbow River decline with downstream distance as a result of biological uptake and dilution from less-enriched lateral inflows (Hensley et al. 2014). Notably, and unlike most other spring-fed rivers in Florida where filamentous algal proliferation is most severe near the head springs, in Rainbow River the abundance of nuisance filamentous algae species appears to increase with downstream

distance (Cowell and Dawes 2008). As early as 1957 Odum noted the "upper zone is characterized by beds of *Sagittaria*, shifting to benthic algae, and visibly increasing turbidity". Thus, this longitudinal spatial pattern in SAV versus algal abundance was likely present even when NO_3^- concentrations were still relatively un-impacted by anthropogenic enrichment. The fact that these spatial patterns existed more than half a century ago even at far lower NO_3^- concentrations, and that we observe a reversed longitudinal relationship where algal abundance in the river is highest in the downstream river where NO_3^- are lowest, makes it hard to invoke NO_3^- as the primary driver of SAV and filamentous algal distribution in Rainbow River. Further, the mass of NO_3^- supplied to the river from the spring vents is approximately 100x what is necessary to satisfy plant and algal demand over the length of the river, challenging the plausibility of N limitation.

Other physical and chemical characteristics of the river which might influence SAV growth and algal abundance include flow velocities, other nutrient concentrations such as phosphorus (P) or iron (Fe), and benthic sediment characteristics. The purpose of this study was to critically examine the NO_3^- enrichment hypothesis, and to explore alternative potential drivers of autotrophic community structure in Rainbow River. We divide this comprehensive report into several sections detailing our efforts. A summary of each section, and the major findings are provided below.

Section 1. River Characterization

We observed SAV and filamentous algal abundance to vary markedly along the length of Rainbow River. Consistent with previous observations, native *Sagittaria kurziana* abundance declines with downstream distance, as did most other SAV species. The notable exception was the invasive *Hydrilla verticillata*. Filamentous algae abundance also increased with downstream distance. Water velocity as a control on downstream export of filamentous algae has been recognized as an important control elsewhere, however in Rainbow River we did not observe significant variation in stream velocities along the length of the river, and site specific filamentous algal abundance was not related to water velocity. Water chemistry also varied markedly along the length of the river. Consistent with previous observations, nitrate (NO_3^-) concentrations decline with downstream distance. In contrast, concentrations of biologically

available phosphorus (OrthoP), particularly in sediment porewaters, increase along the length of the river. This form of phosphorus appears to be derived from natural sedimentary deposits rather than from a new anthropogenic source and corresponds to the lower reaches of Rainbow River which were mined extensively for phosphate minerals a century ago. The positive spatial correlation between filamentous algal abundance and P concentrations (as opposed to NO_3^- where the relation is negative) suggests a potential for P to be an explanatory variable, which we describe in a Section 4. Sediment size generally decreased with downstream distance, with clay-like sediments becoming quite common in the lower river. SAV abundance decreased with decreasing sediment size, while bare patch abundance increased, perhaps suggesting an inability to grow in fine grain sediments, something we explore in Section 5. Notably however, sediment size or porewater chemistry did not appear correlated with filamentous algal abundance.

Section 2. Blue Cove Profiling

A notable feature of the lower Rainbow River is Blue Cove, a remnant phosphate mining pit. There is concern that this flow-through cove represents a source of nutrients or otherwise impairs water quality within the river. To investigate this possibility, we characterized the hydraulics of the cove and performed periodic sampling of inlet and outlet water chemistry. We determined the volume of the cove to be 405,500 m^3 (~107 million gallons) and based on inflows and outflows the residence time ranged from 30-56 hrs (roughly 2 days). Vertical temperature and water chemistry profiles suggest the cove is well mixed (i.e. un-stratified). Outlet concentrations of NO_3^- and Total Phosphorus (TP) were almost always lower than input concentrations suggesting the cove is a net sink for nutrients. However, Chlorophyll A concentrations (a measure of phytoplankton abundance) were often highly elevated in the outlet, suggesting the cove does contribute to reduced water clarity downstream by the export of phytoplankton.

Section 3. River metabolism

To determine whether NO_3^- (or PO_4^{3-}) could potentially contribute to filamentous algal proliferation we sought to determine autotrophic demand for these nutrients. Using both a fixed, time-series approach, and floating longitudinal approach we measured rates of gross primary

production (GPP) and autotrophic nutrient uptake. Both methods gave similar values. GPP averaged around 10 g-O_2/m^2/d. Autotrophic uptake of NO_3^- averaged around 100 mg-N/m^2/d, while autotrophic uptake of PO_4^{3-} averaged around 15 mg-P/m^2/d. Together these rates imply an uptake C:N:P ratio which approximately matches the tissue stoichiometry of the autotroph species. Knowing autotrophic demand, we can compare this to the flux of nutrients available for uptake being transported by the river. Under current concentrations, NO_3^- supply exceeds autotrophic demand by two orders of magnitude (i.e. nearly 100 times more). Even using conservative estimates of historic supply, autotrophic demand could have been met several times over. Thus it appears unlikely that GPP in Rainbow River was ever limited by NO_3^-, something explicitly rejected during Odum's earliest studies more than 50 years ago. We also note that GPP values observed in this study are slightly lower, not higher than those measured historically, though they are from only a two week period. Longer term measurements of ecosystem metabolism, which integrates the activity of all plants and animals and is thus a measure of aggregate system health, in this and other spring-fed rivers are likely to be critical to capture the trajectories of ecological change, and for elucidating the drivers of variation in metabolism and nutrient uptake.

Section 4. Benthic Chamber Nutrient Amendments

To determine how enrichment with NO_3^- and other nutrients might impact rates of GPP, we performed nutrient addition experiments using benthic chambers. These chambers were deployed in sets of four, with one serving as a control, and the other three receiving combinations of NO_3^-, PO_4^{3-} and Iron (Fe^{2+}). GPP within each chamber was measured over a week before all chambers were moved to a new location and reset. While sunlight was strongly predictive of GPP (as it was in Odum's studies), a substantial NO_3^- effect on GPP was not readily apparent. NO_3^- addition did not stimulate GPP or epiphytic algal growth, and we observed no decline in GPP over the course of deployments even though NO_3^- in the control chambers was depleted to roughly historic concentrations over that time. The benthic chamber experiments did suggest that elevated P may inhibit GPP in areas where SAV are dominant. They also suggest that both GPP and epiphytic algal biomass accrual may be stimulated by Fe^{2+} additions, a finding consonant with extremely low Fe^{2+} levels observed throughout the system (and across many spring ecosystems), the much greater Fe^{2+} requirements of filamentous algae vis-à-vis the

submerged macrophyte taxa dominant in springs, and also potentially explaining a compelling negative association previously observed between algal abundance and dissolved oxygen. Further investigation of Fe^{2+} limitation, and mechanisms for spatial and temporal enrichment patterns, emerges as a future management need.

For NO_3^- we were able to continuously monitor uptake over the course of deployments by positioning a continuous sensor inside chambers. The results suggest that while autotrophic uptake of NO_3^- does decline modestly with concentration depletion, the larger effect is on the magnitude of dissimilatory removal (i.e. less excess NO_3^- being denitrified). Furthermore this decline in autotrophic uptake of NO_3^- does not impact GPP (at least over week long deployments), suggesting autotrophs are equally adept at obtaining N from other sources, either by recycling or using an alternative N-species such as ammonium (NH_4^+). The finding that nitrate assimilation and GPP are both largely independent of NO_3^- concentrations is further evidence that reducing loads may not have the desired impact on the plant community.

Section 5. Vegetation Transplants

To test sediment type versus other spatial controls on SAV growth we performed a vegetative transplant study. Across three species (*Sagittaria kurziana, Vallisneria americana* and *Hydrilla verticillata*) we observed minimal differences in growth in upstream versus downstream locations. *S. kurziana* displayed a significant negative growth response to clay sediments, suggesting this may be partially responsible for the longitudinal declines in *S. kurziana* coverage. Notably, no species exhibited any significant difference between high-P native clay and low-P bentonite, suggesting it likely to be an effect of sediment size/textural rather than a geochemical effect. The results suggest that downstream declines in *S. kurziana* are the result of longitudinal variation in sediment characteristics rather than water chemistry.

Conclusions

The results clearly demonstrate that NO_3^- enrichment is unlikely to be the primary driver of the decline in native SAV and proliferation of filamentous algae observed in the lower Rainbow River. This strongly suggests that reduction of NO_3^- loading would not produce substantial changes in autotroph distribution. This is unsurprising, given these spatial patterns in

autotroph distribution are likely to have existed more than half a century ago, before contemporary NO_3^- enrichment was observed. We note that this does not imply that reduction of NO_3^- is not a desirable objective. Preventing contamination of the aquifer protects our primary drinking water source. Excess N not assimilated in the river is ultimately transported downstream to costal estuaries, potentially resulting in eutrophication, harmful algal blooms and hypoxic dead zones. However, it appears unlikely that anything short of a massive reduction of NO_3^- concentrations in the Rainbow River (to below historic values) would produce a direct response in the autotrophic community which is not, and likely never has been N limited. Our results suggest that benthic sediments and/or sediment porewater chemistry likely play an important role in determining SAV coverage, and that longitudinal variation in these parameters may explain SAV spatial patterns. In particular, both profiling of the river, and artificial transplantation suggest that *Sagittaria kurziana* grows poorly in the clay-like sediments which are abundant in the lower Rainbow River. Finally, our results suggest that iron enrichment may play an important role in controlling both primary production and epiphytic algal growth. This emerging evidence for Fe^{2+} limitation may provide new insights about the timing and spatial distribution of ecological changes in Rainbow River and beyond, and should, along with continued monitoring of aggregate ecosystem health based on long-term metabolism measurements, be considered important priorities for future investigations.

Section 1 River Characterization

Introduction

Systematic mapping and monitoring of vegetation in Rainbow River has occurred in 1991 (Water & Air Research 1991), 1996 (FDEP unpublished), 2000 (PBS&J 2000), 2005 (PBS&J 2007), 2011 (Atkins 2011), and 2015 (W&AR 2016). The methods and metrics used in these studies varied, making direct comparisons somewhat difficult. Total submerged aquatic vegetation (SAV) coverage was variable across studies, with no consistent long-term trend readily apparent. Studies which compared with previous results (PBS&J 2007, W&AR 2016) do note a change in the relative composition of the SAV community. Among the more prevalent species they note consistent declines in *Sagittaria kurziana* (still the most prevalent species river-wide) and increases in *Vallisneria americana, Najas guadalupensis* and the invasive *Hydrilla verticillata*. Spatially, *Sagittaria kurziana* remains the dominant species in the upper half of the river, while becoming sparse in the lower half of the river. *Vallisneria americana* is most common in the middle portion of the river, while the lower river is dominated by *Hydrilla verticillata*. Filamentous algal cover (either as a benthic mat or attached to other SAV species) increases substantially with downstream distance, from less than 20% in upper reaches of the river to nearly 70% in lower reaches (W&AR 2016). Our purpose here was to characterize longitudinal patterns in vegetation as well as longitudinal trends in water chemistry and sediment characteristics which might explain the observed vegetation patterns, and in particular, the increase in benthic filamentous algae associated with the lower river.

Methods

We conducted a survey of aquatic vegetation along the length of Rainbow River beginning on September 24th and concluding on October 29th 2014. Twenty-four transects were performed, spaced at roughly 400 meter intervals from the headspring to the confluence with the Withlacoochee River. The latitude and longitude of each transect is provided in Table1-1.

Along each transect, 3-5 sites (depending on channel width) were selected for profiling using a one meter square quadrat which was randomly dropped over the side of the boat. Using a

mask and snorkel, percent vegetative cover within the quadrat was ascribed to one of seven cover classes using reference tables. Cover classes were 0%, 1-10%, 10-25%, 25-50%, 50-75%, 75-90% and 95-100%. The species present were identified and the height of the vegetation or filamentous algae mat was recorded using a meter stick. Underwater photos of each site were taken for future reference.

Table 1-1. Transect locations.

Transect #	Latitude	Longitude	Transect #	Latitude	Longitude
1	29.1017	-82.4371	13	29.0535	-82.4476
2	29.0767	-82.4276	14	29.0500	-82.4479
3	29.0733	-82.4265	15	29.0467	-82.4491
4	29.0698	-82.4270	16	29.0457	-82.4523
5	29.0663	-82.4273	17	29.0457	-82.4564
6	29.0629	-82.4281	18	29.0951	-82.4343
7	29.0617	-82.4319	19	29.0928	-82.4313
8	29.0608	-82.4358	20	29.0928	-82.4273
9	29.0601	-82.4396	21	29.0898	-82.4262
10	29.0589	-82.4434	22	29.0869	-82.4285
11	29.0564	-82.4456	23	29.0833	-82.4287
12	29.0983	-82.4361	24	29.0802	-82.4280

At each site we collected sediment pore water samples. Pore water was extracted using a 30cm long perforated aluminum probe that was inserted into the sediment. Rubber tubing connected the probe to a peristaltic pump. Dissolved Oxygen was measured in the field using an in-line HOBO DO sensor (Onset, Bourne MA). Water samples were passed through a 45 micron filter in the field and stored on ice. Samples were sent to the University of Florida Analytical Research laboratory for analysis of dissolved inorganic carbon (DIC), dissolved organic carbon (DOC), Potassium (K), Calcium (Ca), Manganese (Mn), Iron (Fe), Magnesium (Mg), ammonium (NH_4-N), nitrate (NO_3-N), nitrite (NO_2-N), Total Kjeldahl nitrogen (TKN), and orthophosphate (PO_4^{3-}). Porewater concentrations were compared to surface water concentrations collected at roughly the same time as part of SWFWMD's quarterly water quality sampling.

At each site we measured water velocity halfway between the surface and the bottom, using an acoustic Dopper velocimeter (SonTek, San Diego CA). Water depth was measured using a weighted tape. Sediment depths were measured using a steel tile probe fitted with a slide hammer. For logistical reasons, we used a sediment depth of 2.5 meters as a maximum cutoff, reasoning sediments beyond this depth were likely to exert little influence on overlying vegetation. At each site we collected sediment samples using a piston corer. Sediment samples

were analyzed for composition, particle size and organic matter content. Particle size analysis was performed using a hydrometer to separate sediments into three size classes, sand (d>0.05 mm), silt (0.002<d<0.05 mm), and clay (d<0.002 mm). Percent organic matter was determined by loss on ignition by combusting for 9 hours at 350˚C.

Results

Average percent cover of each species at each transect is shown in Figure 1-1. Although our measurement methods differed substantially, our results appear generally comparable to those collected in 2011 (Atkins 2011). W&AR's profiling in summer 2015 suggested significant increases in vascular vegetation since the 2011 SAV evaluation, and our results suggests this may primarily have occurred over the relatively short period following our profiling in fall 2014 (roughly 9 months prior). While differences in methodology exist between the 2000 to 2015 SAV surveys (including improvements in GPS and GIS technology), and the nature of random sampling adds a large degree of uncertainty, we believe it is safe to characterize the distribution of vegetation in Rainbow River as rather dynamic, and capable of measurably changing over relatively short periods of time.

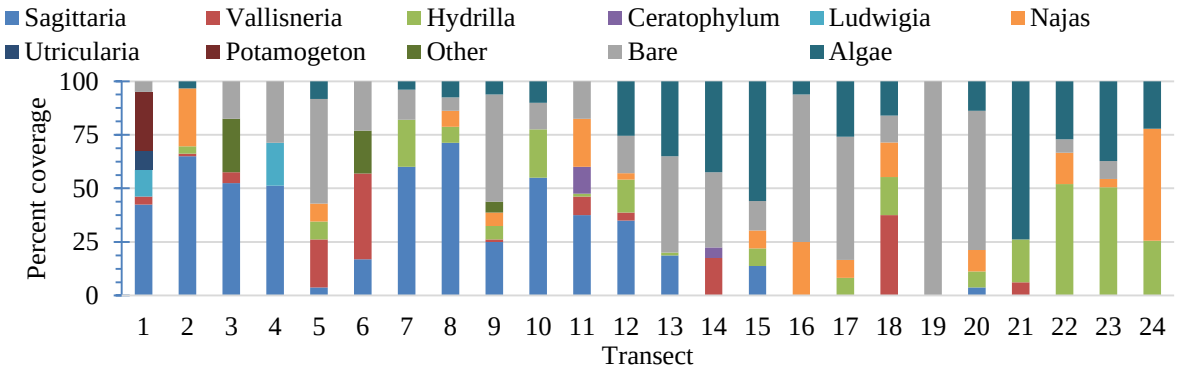

Figure 1-1. Average percentage of vascular SAV cover for each transect generally declines with downstream distance (with the exception of exotic Hydrilla) while percent algal cover generally increased.

As with previous studies, we noted a marked longitudinal transition in the autotroph community structure (Figure 1-2). The upper river is dominated by vascular plants, primarily *Sagittaria kurziana*. There is a substantial decline in vascular vegetation with downstream distance, and filamentous algae, predominantly *Lyngbya wollei*, becomes the dominant autotroph

(mixed in with invasive *Hydrilla verticillata*). The prevalence of bare patches also increases with downstream distance (though not statistically significant).

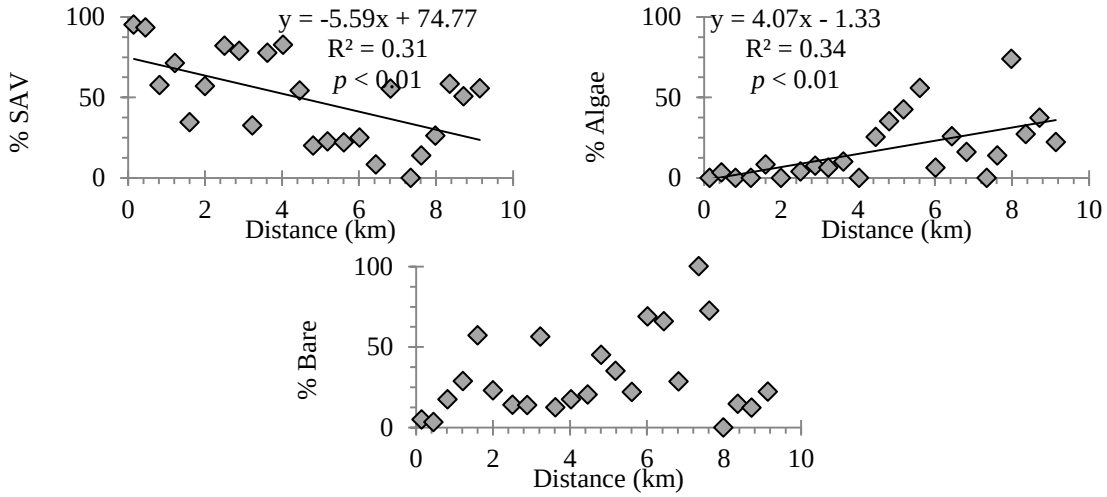

Figure 1-2. Longitudinal trends of benthic cover type, averaged across transects.

We observed porewater chemistry to be vastly different from surface water chemistry. We also noted longitudinal trends in porewater chemistry for several species. We note that in nearly all locations NOx-N is depleted in the pore water relative to the surface water (Figure 1-3), likely as a result of denitrification. This suggests water emanating directly from springs to be the primary source of NOx-N rather than diffuse seepage out of the hyporheic sediments. Based on the observed longitudinal declines in surface water NOx-N, sediments are likely a sink (location of denitrification). Porewater was enriched in NH_4-N relative to the surface water, and porewater concentrations increase with downstream distance. This suggests the hyporheic zone may be a source of NH_4-N to the river channel. Rapid nitrification of NH_4^+ into NO_3^- in oxic surface waters, potentially explains why surface water NH_4-N remains low. Porewater OrthoP concentrations were also heavily enriched relative to the surface water, and also increased with downstream distance, suggesting hyporheic sediments are a major source of OrthoP to the river channel. Extremely high porewater OrthoP concentrations in the lower river correspond with locations which in the past were mined for phosphorus. Porewater DIC, K^+ and Ca^{2+} were also elevated relative to surface water concentrations, and also increased with downstream distance. Fe and Mn concentrations in all samples collected were below detection limits (0.01 mg/L) for instruments used by the lab.

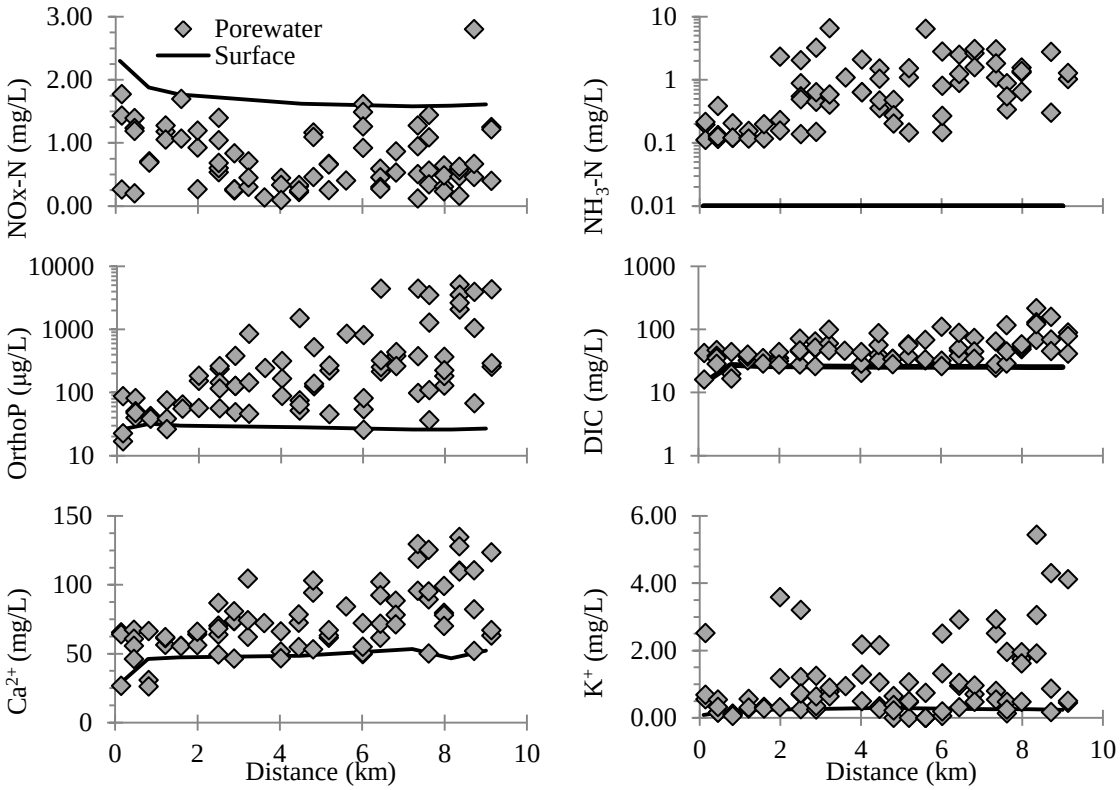

Figure 1-3. Longitudinal profiles of porewater measurements (points). Surface water measurements from SWFWMD quarterly profiling are also shown (lines).

Sediment composition varied markedly with downstream distance (Figure 1-4). Sediment P increased by two orders of magnitude. High P sediments in the lower river are unsurprising, given in the past these sediments were mined for phosphate. These sediments likely represent the source of the elevated downstream pore water dissolved P concentrations. Sediment Ca also showed a longitudinal trend, increasing in the lower river. Apatite (calcium phosphate) is a common mineral form of phosphate. The percent Ca versus percent P observed in downstream sediments suggests a ratio of roughly 4:1, which is slightly higher than the molar ratio of Ca to P in the calcium phosphate mineral apatite (10:4). Additional calcium bearing minerals including calcium carbonate (limestone) may also be present. Despite being below detection limits in water samples, sediment Fe and Mn also exhibited marked longitudinal increases. Finally, despite longitudinal increasing NH_4-N in porewater samples, sediment TKN exhibited no spatial trend.

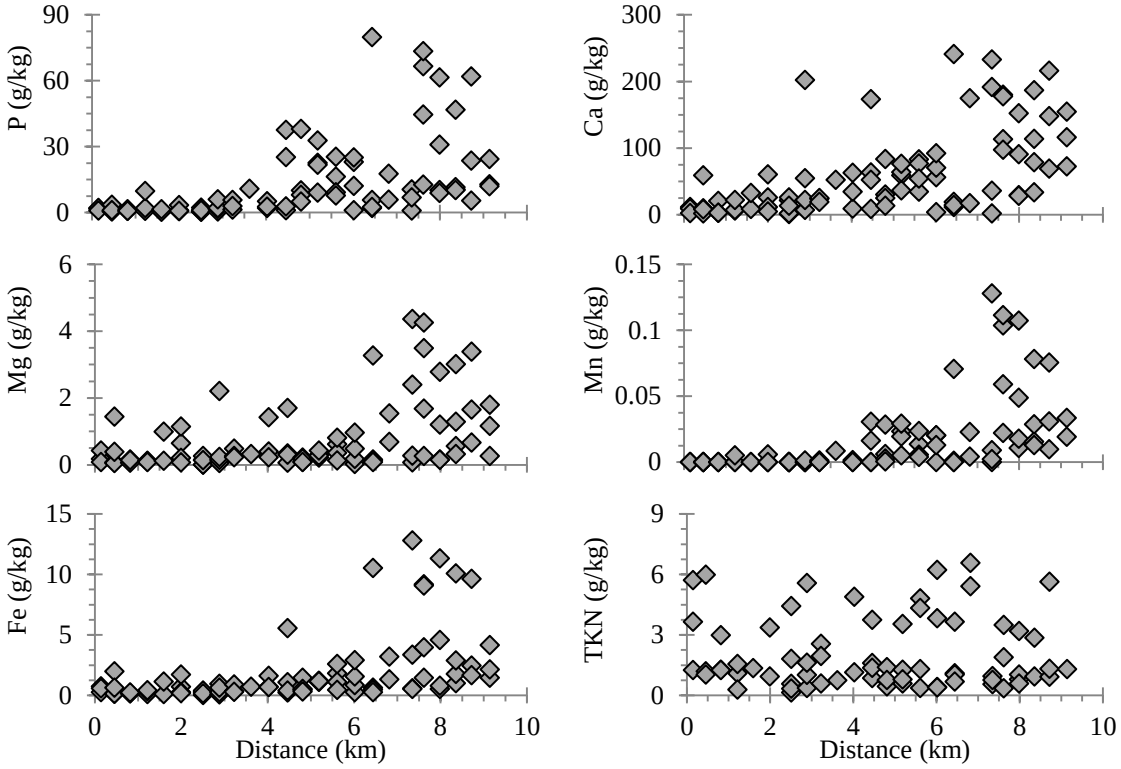

Figure 1-4. Longitudinal profiles of sediment elemental composition.

Sediment particle size also exhibited longitudinal patterns. We observed a decrease in the fraction of sand with downstream distance, and a corresponding increase in silt and clay (Figure 1-5). Percent OM did not show a significant longitudinal trend.

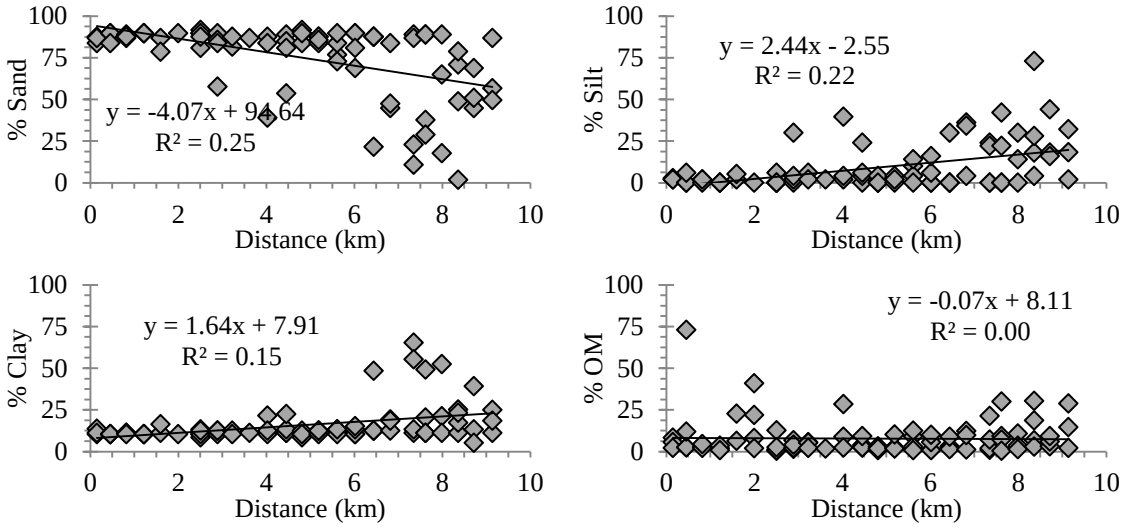

Figure 1-5. Longitudinal profiles of sediment size (sand d>0.05 mm, silt 0.002<d<0.05 mm, and clay d<0.002 mm) and percent organic matter (across all size classes).

While longitudinal trends in sediment particle size were noticeable, laterally across the channel we did not observe any significant trends in sediment size or percent OM (Figure 1-6).

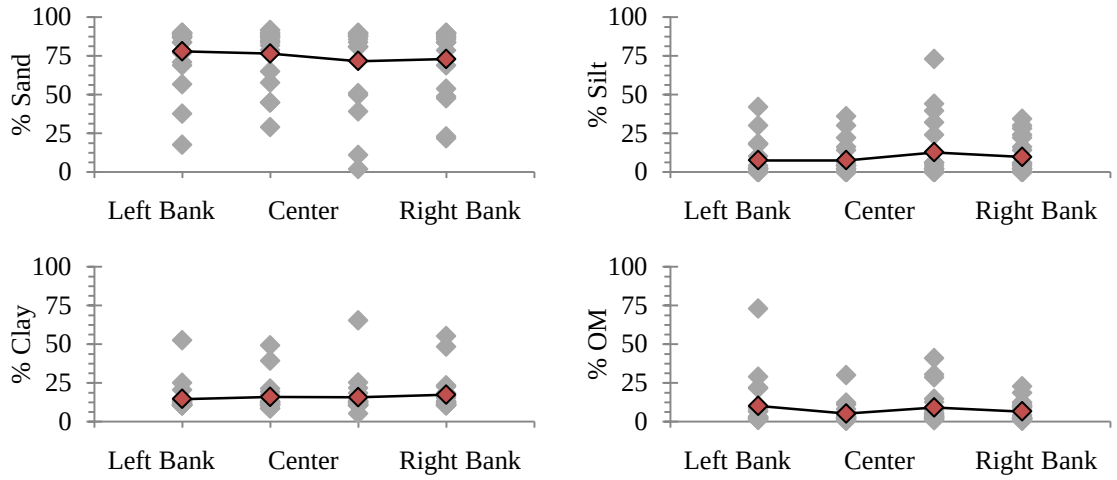

Figure 1-6. Lateral profiles of sediment size and percent organic matter. Red points indicate means.

Differences in sediment particle size may arise due to stream hydraulics, with finer sediments being entrained in higher velocity areas. However, in our longitudinal assessment we observed no significant longitudinal trends in surface velocity (Figure 1-7). Previous work (Hensley et al. 2012) suggested that the lower river becomes narrower, with potentially higher velocities (though it's important to note this single tracer test was carried out under a single set of hydraulic conditions). Laterally, there was a strong velocity gradient, with higher velocities in the center of the channel (Figure 1-7), however this did not appear to affect the distribution of sediment size across the channel. Thus sediment particle size does not appear to be substantially correlated with velocities, either longitudinally or laterally. An alternative is that sediment size is more related to underlying geology than surface velocity. X-ray crystallography shows the clay sediments to be composed almost exclusively of colloidal apatite.

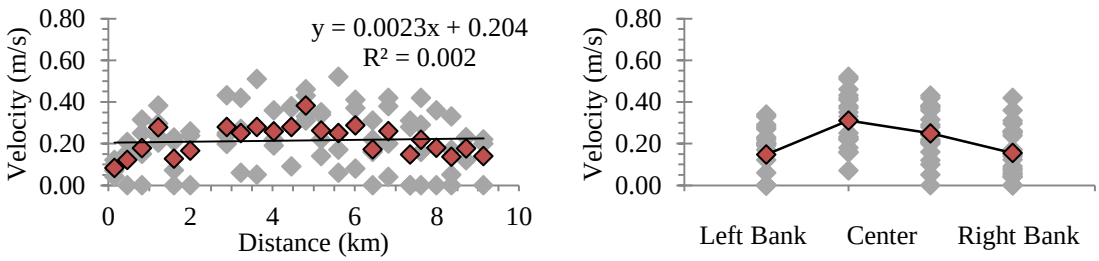

Figure 1-7 Longitudinal (left) and lateral (right) velocity profiles. Red points indicate means.

We did not observe any statistical correlation between benthic cover type and water velocity, either treating sites independently, or averaging sites across transects (Figure 1-8).

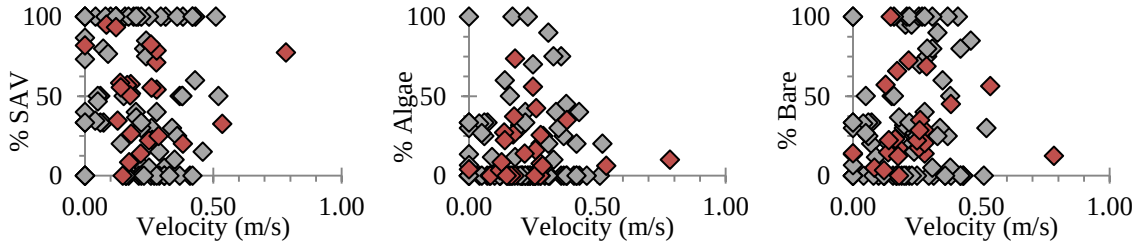

Figure 1-8 Benthic cover type versus water velocity. Gray points are individual sites, red points are transect means.

Considering individual sites, benthic cover type was not correlated with sediment size. However, when averaging across transects sediment size and vascular SAV declined with downstream distance while percent filamentous algae and percent bare increased. Across transects, average vascular SAV cover exhibited a strong negative correlation ($p < 0.01$) with average percent clay sediments while average percent bare was positively correlated ($p = 0.04$) with average percent clay sediments (Figure 1-9). This suggests that sediment texture may play a role in the distribution of vegetated versus bare patches, though it is important to remember that correlation does not confirm causation, and other ancillary factors may be at work. This is particularly true given we observed this effect at the transect level, but not the site level.

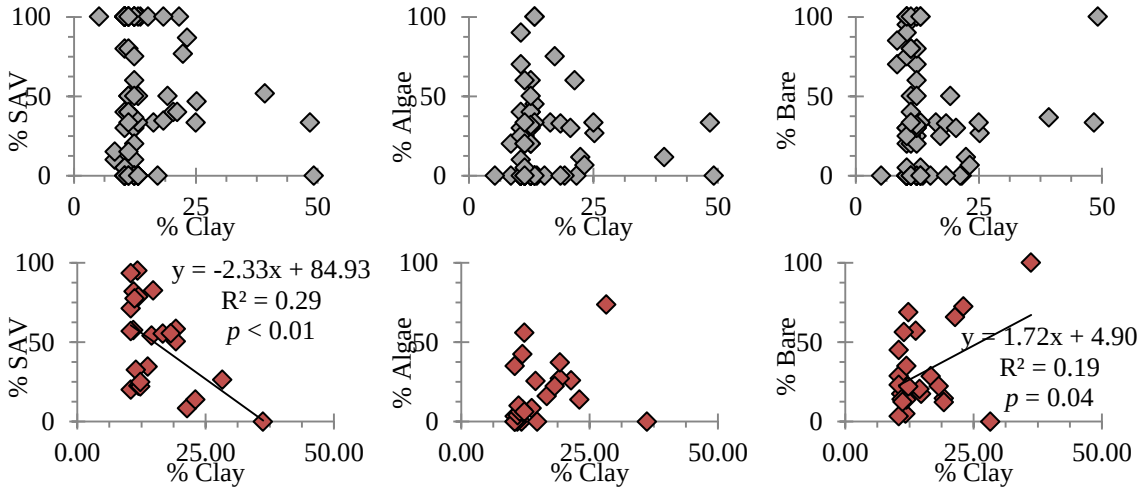

Figure 1-9. Benthic cover typer versus sediment percent clay for individual sites (top row) and transect averages (bottom row). At the transect level percent vascular SAV was negatively correlated with average sediemnt percent clay while percent bare was negatively correlated with average percent clay.

One of these ancillary factors may be porewater chemistry, wich also exhibited strong longitudinal trends. As with velocity and sediment size, we did not observe statistically significant effect at the site level. However averaging across transects we observe a strong negative crrelation between SAV cover and porewater OrthoP concentrations (Figure 1-10). It is impossible using this dataset to say whether these relationships are diven by sediment texture or porewater chemistry. For this reason we performed the controlled vegetation transplant study in Section 5.

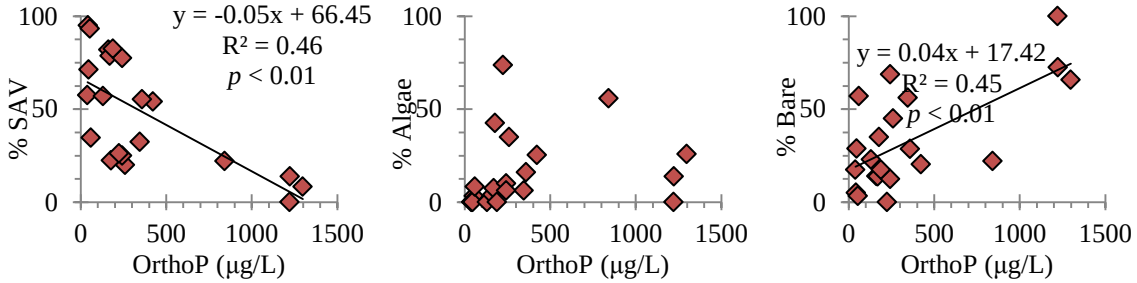

Figure 1-10. Benthic cover type versus porewater OrthoP, averaged across transects.

Section 2. Blue Cove Profiling

Introduction

The lower Rainbow River features several large, flow-through coves. Beginning in 1889, the lower Rainbow River was the site of extensive phosphate mining, turning nearby Dunnellon into a boom town. These coves, as well as the deeper areas downstream of the Highway 484 bridge, are the remnants of phosphate mining activities. There has been concern that these coves may significantly impact water chemistry and water clarity within Rainbow River. Our purpose was to determine whether the coves represent a net source or sink for nutrients to the river, and the impact of the coves on downstream water clarity.

Initial profiling suggests that the residence time of Little Blue Cove on the east side of the river is on the order of half a day, likely too short for it to exert significant influence. This is supported by outlet TP, NO_3^- and ChlA concentrations which are nearly identical to inlet concentrations. We therefore chose to focus our continued efforts on the larger Blue Cove located on the west side of the river. This cove is large enough that it likely has a turnover time of 2 days or more, sufficient time for phytoplankton accumulation to occur.

Methods

Exchange rates were estimated by measuring inflow/outflow using the USGS cross-sectional method. Velocities and depths were measured at 2-3 meter increments across the inlets and outlets to the coves. Depths were measured using a pressure transducer, while velocities were measured using a Lorentz velocimeter (which measures the distortion of an electromagnetic field by a fluid in motion). For depths less than 1 m velocities were measured at 0.6*depth, while for depths greater than 1 m velocities were measured at 0.2*depth and 0.8*depth and averaged. Cove area was estimated using areal imagery, and average depth was determined by taking several soundings using a weighted tape. The estimated volume of each cove was then calculated by multiplying the estimated area by the average depth. The estimated turnover time was calculated by dividing the estimated cove volume by the estimated exchange rate.

Water samples at the inlet and outlet were periodically collected and analyzed for OrthoP, NO_3-N, NH_4-N and ChlA. In-situ fluorometers (Turner C3; Sunnyvale CA) were positioned at the inlet and outlet of the larger cove to record continuously at 15-min sampling intervals over 2, week-long deployments. Fluorescence readings were calibrated using ChlA samples collected at the beginning and end of each deployment. Within Blue Cove, we established 4 stations, one in each of the three "lobes" and one directly in the center (Figure 2-1). At each of these stations were periodically collected Secchi disk readings. Using an EXO sonde (Yellow Springs OH) we collected vertical profiles of temperature, DO, specific conductance and pH. Using a peristaltic pump, we collected water samples from multiple depths which were then analyzed for OrthoP, NO_3-N and NH_4-N.

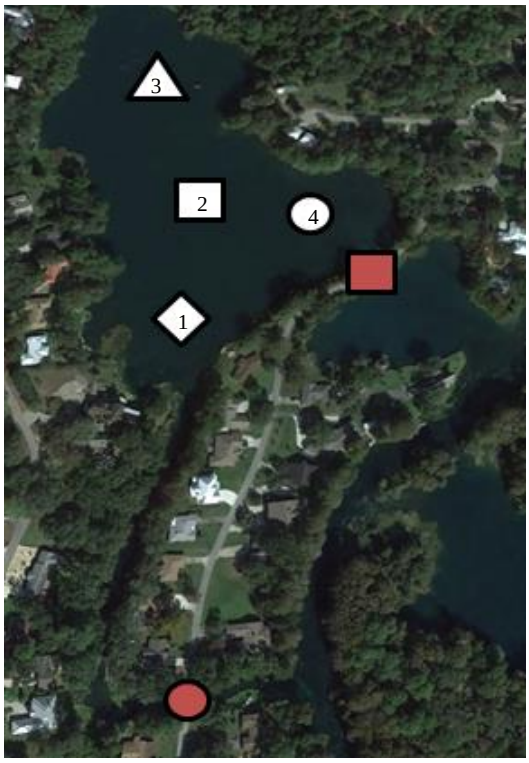

Figure 2-1. Locations of inlet (red square), outlet (red circle) and sampling locations (white) for Blue Cove.

Results

A summary of measured Blue Cove inflow and outflow is shown in Table 2-1. We note that on each date outflow was slightly larger than inflow, suggesting there may be an additional source of water to the cove.

Table 2-1 Blue Cove Inflow/Outflow (m^3/s)

Date	Inflow	Outflow
3/18/2014	1.98	2.11
6/11/2014	1.78	1.96
6/18/2015	1.85	2.04
6/25/2015	2.04	2.19
10/6/2015	3.58	3.96
3/31/2016	2.36	2.41

A summary of Blue Cove bathymetry and turnover time is shown in Table 2-2. The range in turnover time is based on the minimum and maximum measured exchange rates.

Table 2-2 Blue Cove Bathymetry

Parameter	Value	Units
Area	45,000	m^2
Average depth	9	m
Volume	405,500	m^3
Turnover time	30-56	hrs

A summary of Secchi depth measurements at each of the sampling locations is shown in Table 2-3. Note that vertical Secchi depths could not be taken at the inlet and outlet because of the limited water depth. Measurements at location 1 also sometimes reached the bottom (noted as > 4 m). We note that Secchi depths are generally greatest closer to the inlet (site 4).

Table 2-3 Summary of Blue Cove Secchi Depths

	Location				
Date	4	3	2	1	Units
3/18/2014	2.0	2.3	2.1	1.9	m
10/6/2015	4.0	3.6	3.6	>4.0	m
3/31/2016	5.8	5.1	5.4	>4.0	m

Vertical profiles of water chemistry parameters are shown in Figure 2-2. We note several important trends. While there is no evidence of complete thermal stratification, there are vertical temperature gradients, with bottom temperatures closely matching those of the inlet (i.e. spring water which is average ground temperature), while surface temperatures are elevated, particularly on the warm day of 10/6/2015. Surface temperatures were most elevated at sites 2 and 3, those furthest from the direct path between the inlet and the outlet.

Dissolved Oxygen was higher at the outlet than at the inlet, consistent with both re-aeration of under-saturated spring water and net primary production within the water column of the cove. DO decreased slightly with depth. We note that on both dates we have data for, DO at the bottom of site 1 was noticeably lower than in any other location. We noted that this site was shallower than the rest (4 m versus 8+ m at other sites) such that light was often able to reach all the way to the bottom under most Secchi conditions, and we noticed the presence of a thick filamentous algae mat.

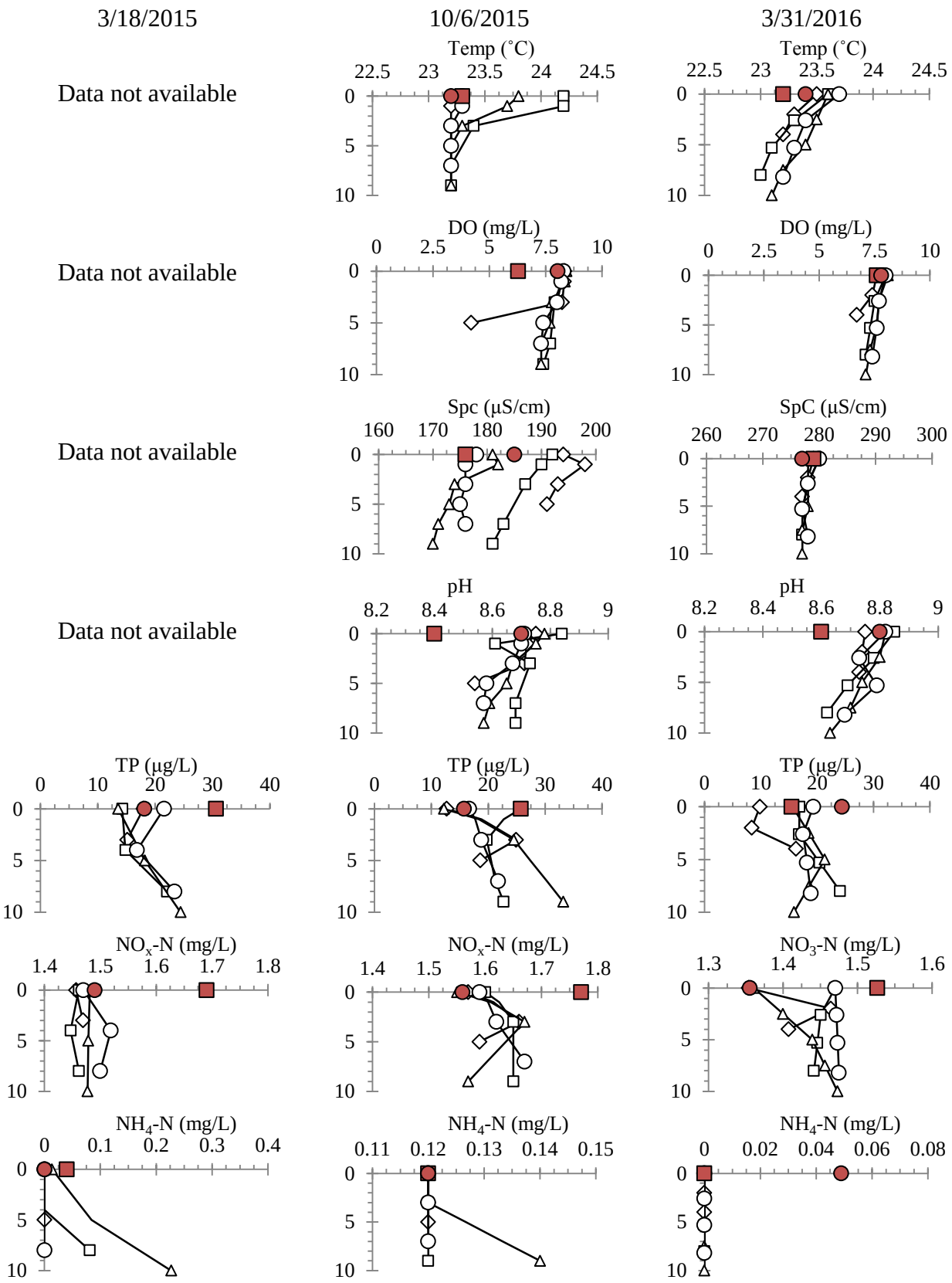

Figure 2-2. Vertical profiles of water chemistry parameter. Y-axis is depth in meters.

Table 2-4. Summary of Blue Cove inlet and outlet TP, NH_3-N and NH_4-N concentrations.

Date	TP (µg/L)		NOx-N (mg/L)		NH_4-N (mg/L)	
	Inlet	Outlet	Inlet	Outlet	Inlet	Outlet
3/18/2015	28.36	18.1	1.69	1.49	0.00	0.00
6/11/2015	24.32	16.04	1.57	1.33	-	-
6/18/2015	20.29	15.52	1.59	1.33	-	-
6/25/2015	18.23	5.32	1.58	1.34	-	-
7/2/2015	21.14	17.68	1.66	1.43	-	-
10/6/2015	27.51	16.88	1.77	1.56	0.12	0.12
3/31/2016	15.46	24.39	1.53	1.36	0.00	0.05

TP concentrations were typically lower at the outlet relative to the inlet, suggesting the cove is a net sink for dissolved P. For March 2016, when outlet TP concentrations appear enriched relative to the inlet, this is the only instance where outlet concentration (of any solute) was substantially different that surface water concentrations within the cove, suggest this measurement may possibly be erroneous. TP concentrations generally increased with depth in the water column, consistent with a sediment source. We note TP concentrations were often highest at site 3, which is the deepest location in the cove presumably because it was the most heavily excavated, suggesting it may once have contained a large localized phosphate deposit.

NO_x-N concentrations were also noticeably lower at the outlet relative to the inlet, suggesting the cove is a net sink for NO_3^-. We did not note any consistent vertical trends to suggest denitrification within the water column, not surprising given the DO profile which suggests aerobic conditions throughput. Concentrations at all sites were quite similar to the outlet concentration, suggesting that the cove is well mixed.

NH_4-N was generally close to the detection limit in all profiles and we hesitate to draw any conclusions regarding it. On exception is the bottom at site 3 which consistently showed enriched concentrations, and was also the location where we saw substantial TP enrichment.

ChlA samples from the inlet and outlet of Blue Cove are shown in Table 2-5. Outlet concentrations are noticeably higher than inlet concentrations, suggesting the cove is a source of ChlA to the river. Outlet concentrations in this range would typically be classified as mesotrophic. Using a flow-weighted average (roughly 20% of river flow is diverted through Blue Cove), expected ChlA concentrations in the river downstream of the outlet of Blue Cove would be on the order of 2-3 µg/L. Using these ChlA values, we created a calibration curve for our continuous fluorescence measurements shown in Figure 2-3 below. Figure 2-4 shows continuous measurements of ChlA at the inlet and outlet of each cove (calibrated to units of µg/L). The cove is clearly a net source of ChlA to the river. Interestingly the outlet signal appears to vary on a semi-diurnal cycle, with highest concentrations in the morning and evening, suggesting mid-day inhibition of water column algae, perhaps from UV light.

Table 2-5 ChlA (µg/L)

Date	Inlet	Outlet
6/11/2015	0	9
6/18/15	1	6
6/25/15	1	13
7/2/15	1	12

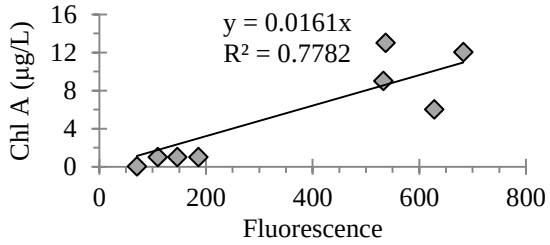

Figure 2-3 ChlA versus fluorescence

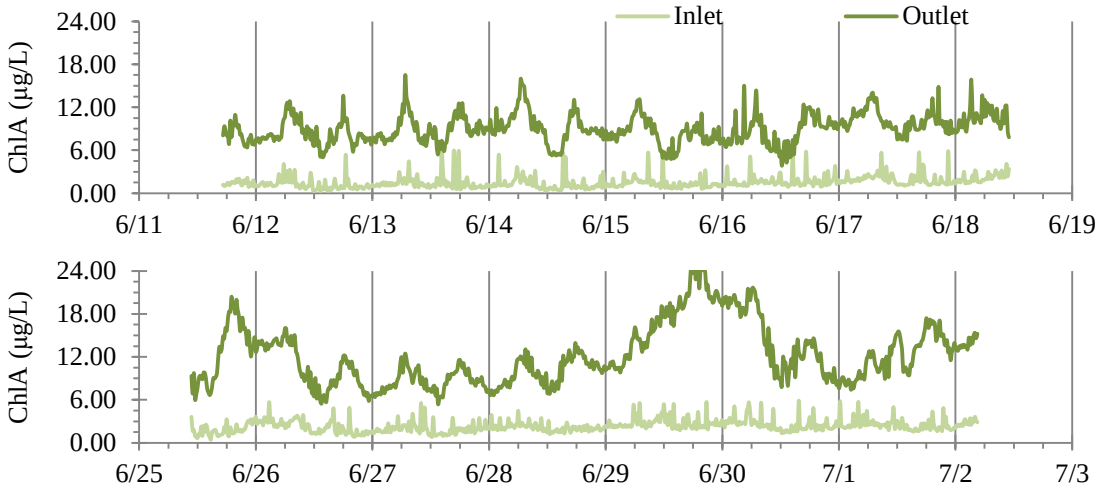

Figure 2-4 ChlA concentrations at Blue Cove inlet (gray) and outlet (black).

Over the course of the sampling, Secchi depth measurements increased from around 2 m in March 2015 to around 3m in October to around 5m in March 2016. During that time

exchange with the river have increased and then decreased again. Across all sampling periods, Blue Cove exchange rates appear strongly correlated with Rainbow River stage (from USGS gage 02313100) (Figure 2-5a). The correlation between exchange and Rainbow River discharge was only weakly significant (p = 0.06; Figure 2-5b). Exchange rate was not a significant predictor of ChlA or Secchi depth (Figure 2-5c and d).

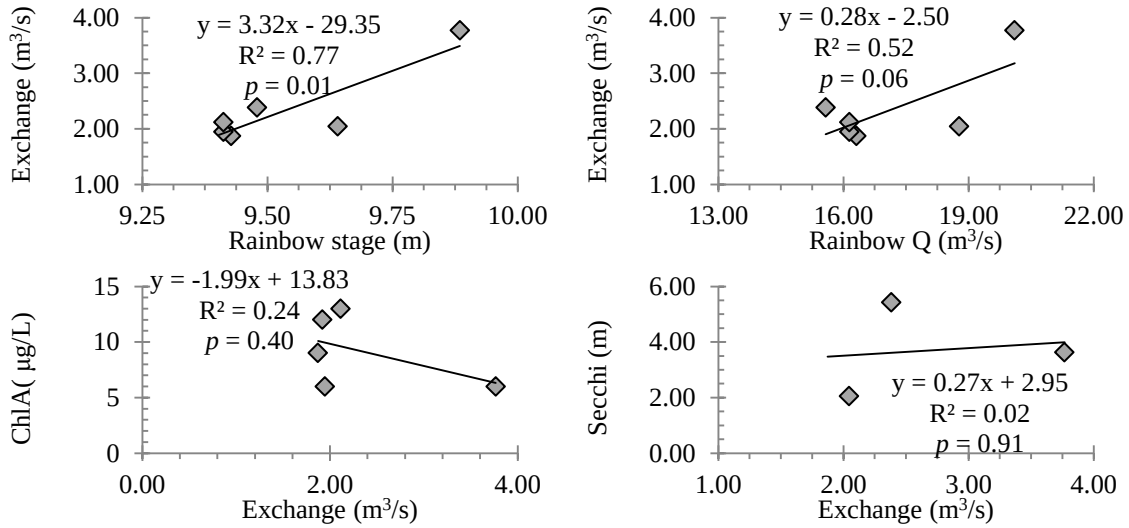

Figure 2-5. Regression of Blue Cove exchange rate versus Rainbow River stage (top left) and discharge (top right). ChlA concentrations and average Secchi depths within Blue Cove do not appear correlated with exchange.

In summary, Blue Cove represents a sink for dissolved nutrients, with outlet concentrations of NO_3- reduced by approximately 0.2-0.25 mg/L relative to inlet concentrations, and outlet concentrations of TP reduced by approximately 5-10 µg/L relative to inlet concentrations (ignoring the March 2016 sample for reasons outlined above). However the cove is a source of reduced water clarity in the form of ChlA, which is negligible at the inlet, but may reach 13 µg/L at the outlet. If we approximate flow through the cove as between 10-20% of the total flow in Rainbow River, this would constitute an increase in river ChlA downstream of the cove of between 1.3 and 2.6 µg/L.

Section 3. Metabolism and ecosystem stoichiometry

Introduction

A method for illuminating the potential for a nutrient such as nitrogen or phosphorus to control primary productivity, is to measure autotrophic demand for that nutrient relative to supply. In the past, measuring nutrient uptake was traditionally done using radio-labeled isotopes which is completely impractical in Rainbow River or any other river of similar size (Ensign and Doyle 2006, Tank et al. 2008). The high-precision, high-frequency datasets generated by recently developed in-situ sensors allows a passive, mass balance approach (Heffernan and Cohen 2010, Cohen et al. 2013). Here we use these sensors to measure both primary production and nutrient uptake rates within Rainbow River, and to estimate the autotrophic demand for nitrogen and phosphorus.

River systems can be viewed using alternative reference frames (Doyle and Ensign 2009). An Eulerian approach tracking changes in the flux of particles through a fixed reference frame with respect to time is more common. However river systems are equally suitable for a Lagrangian approach tracking changes within water parcels as they move through space. For example nutrient uptake rates can be estimated from rates of longitudinal declines (Hensley et al. 2014). Here, we take both approaches.

Methods

Two monitoring stations were established. The upstream station at the location of the USGS station 02313098, just upstream of the State Park tube takeout. The downstream station was located just upstream of the inlet to Blue Cove. These stations thus divided the river into a 4 km upstream and 3.1 km downstream reach. This partitioning of reaches was based on the previous longitudinal characterization (Part 1) which suggested it approximately marked a transition between the dominance of vascular vegetation and filamentous algae. We wanted to determine whether there were noticeable differences in metabolism and relative rates of elemental cycling as a result of this change in primary producer community.

At each station we deployed a HOBO DO sensor (Onset, Bourne MA), a SUNA NO_3^- sensor (Satlantic, Halifax NS), a Cycle-P SRP sensor (Wetlabs, Philomath OR), and a fluorometer (Turner, Sunnyvale CA) for measuring CDOM and ChlA. Additionally, at the upstream station we deployed a dissolved CO_2 sensor and a light meter. The sampling interval was hourly for the Cycle-P and 15 minutes for all other sensors. The deployment lasted 14 days, From December 7 until December 21. Q measurements were obtained from the USGS Water Information Portal (http://waterdata.usgs.gov). Channel cross sectional areas (from Hensley et al. 2012) were then used to estimate mean travel time for offsetting upstream-downstream signals. Using the magnitude of diel variation, we were able to calculate the magnitude of gross primary production (GPP), ecosystem respiration (ER), assimilatory N uptake (U_{A-N}), and assimilatory P uptake (U_{A-P}) for both the upstream and downstream reach using the methods of Heffernan and Cohen 2010 and Cohen et al. 2013. We assumed net primary production was equal to half GPP (Hall and Tank 2003; Hall and Beaulieu 2013). Using NPP, U_{A-N} and U_{A-P} we calculated ecosystem C:N, C:P and N:P ratios for both reaches and compared these to estimates of autotroph tissue stoichiometry found in the literature. Autotroph tissue stoichiometry, arranged by species, is shown in Table 1-2 below. Hydrilla values come from Zimba et al. 1993, all others from Nifong et al. 2014. Note the generally lower C:N ratios in filamentous algal species, while C:P varied marked across species.

Table 3-1 Autotroph tissue molar stoichiometry

Species	C:N	C:P	N:P
Lyngbya	7.7±0.6	387±37	51.4±5.7
Vaucheria	8.9±0.3	539±59	54.4±5.5
Hydrilla	11.1	438	39.3
Sagittaria	15.4±0.8	485±59	31.7±3.7
Vallisneria	18.5±0.9	391±32	21.7±2.5

Longitudinal profiling took place on July 16, 2016. We sampled water chemistry, measuring Temperature, DO, CO_2, SpC, pH and NO_3^-. Nitrate was measured using a SUNA (Satlantic, Halifax NS) sampling in continuous mode every 2 seconds. All other parameters were measured at 2 minute intervals using stand-alone sensors (Campbell Scientific, Logan UT; Vaisala, Vantaa Finland) wired to a data logger. Sensors were attached to a steel support structure suspended over the side of an 18 foot motorized skiff and submerged approximately 0.5 m deep.

The morning profile (10:50-12:45) was collected travelling in an upstream direction from the Withlacoochee River to the headsprings, while the afternoon profile (12:45-14:05) was collected travelling in the opposite direction. A handheld GPS (Garmin, Olathe KS), continuously recorded the track, and was then used to determine the location of each measurement. Uptake rates are calculated using the longitudinal rate of change in concentration.

Results

At both stations we observed strong diel signals across all solutes, consistent with autotrophic forcing. The upstream and downstream signals of each solute are shown in the figure below.

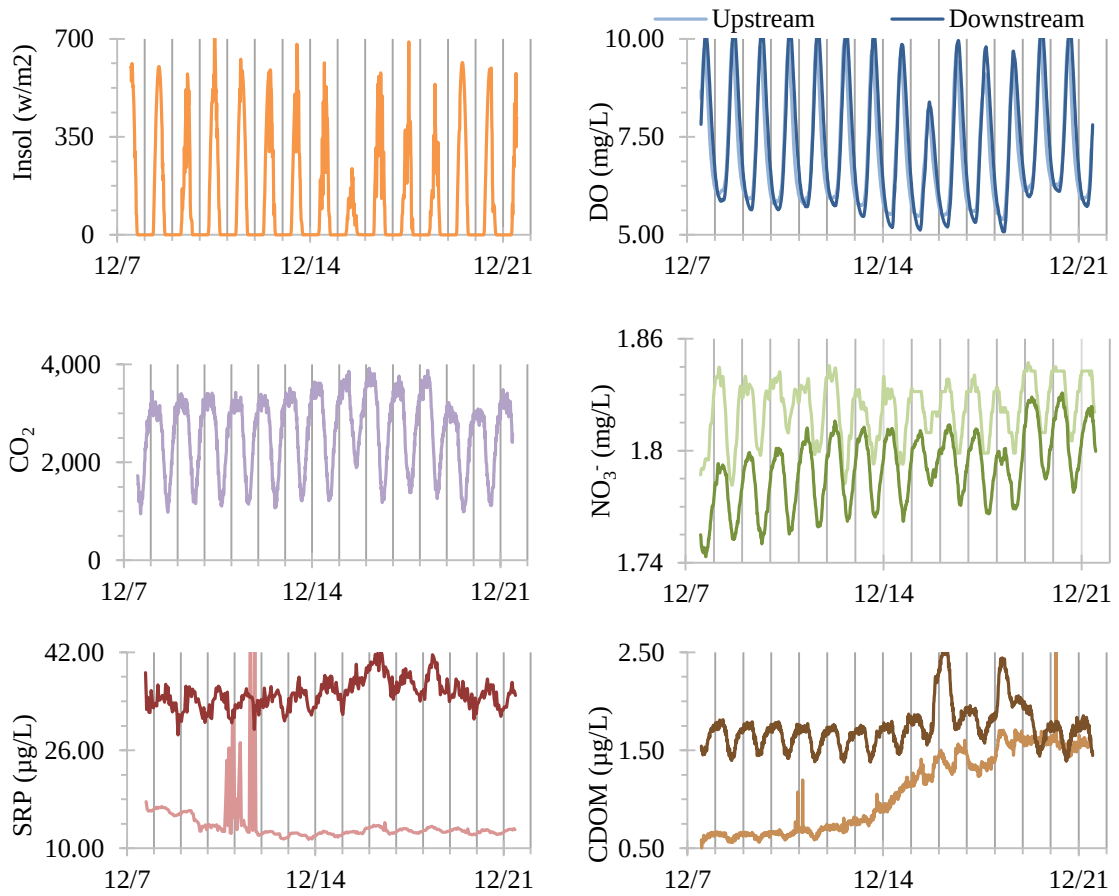

Figure 3-2 Upstream and downstream solute signals.

While estimated values of GPP, ER and $U_{A\text{-}N}$ were reasonable, diel SRP variation at the upstream station was quite modest, and the magnitude of assimilatory P uptake implied by the raw signal in the upstream reach was far too small to give reasonable estimates of C:P (in the

range of 2000-3000). We have observed this phenomenon before (Cohen et al. 2013a), and believe that the majority of the assimilatory P signal is being lost to P co-precipitation with calcite (House 1990), a process which is also time varying as Ca^{2+} saturation changes with diel variation in pH (as a result of consumption/ production of CO_2 through photosynthesis/respiration). In short, daily peak SRP concentrations (which generally occur shortly before mid-day) become truncated because some of this SRP binds to Ca^{2+} as it precipitates out during the day (pH is higher during the day due to consumption of CO_2 through photosynthesis). By using specific conductance as a proxy for Ca^{2+} concentrations, we can calculate how much P is co-precipitating. We then calculated this additional mass which must be added back to the P signal. For a detailed explanation see Cohen et al. 2013a.

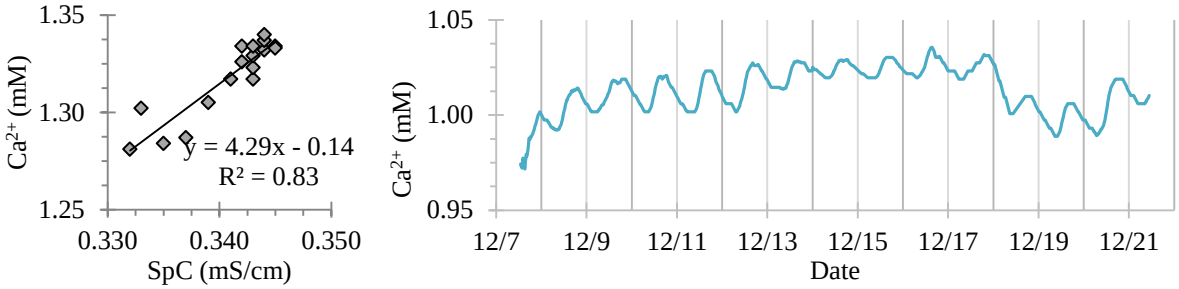

Figure 3-3. Ca^{2+} versus SpC relationship (left) was used to estimate Ca^{2+} concentrations (right).

This significantly increases the diel amplitude (and by extension inferred autotrophic uptake) of the upstream signal such that it is comparable to the downstream signal. Autotrophic uptake is then calculated as the area between the diel signal and a baseline interpolated across daily maximum values. The effect of phosphorus co-precipitation with Ca^{2+} is much larger for the upstream reach because spring water emerges from the aquifer oversaturated with Ca^{2+} which then precipitates out until equilibrium is reached. The downstream station signal gave reasonable estimates without a Ca^{2+} correction, and in any event we did not have a conductivity sensor stationed at the downstream station to make the analysis possible.

It is interesting to note that daily maximum P uptake (lowest concentration) occurs several hours later in the day than maximum primary production or NO_3^- assimilation, something previously noted in the Ichetucknee (Cohen et al. 2013a) and interpreted as asynchronous metabolic uptake of different elements. There is evidence to suggest that RNA production, which utilized PO_4^- as a "backbone", peaks at night (Lepp and Schmidt. 1998).

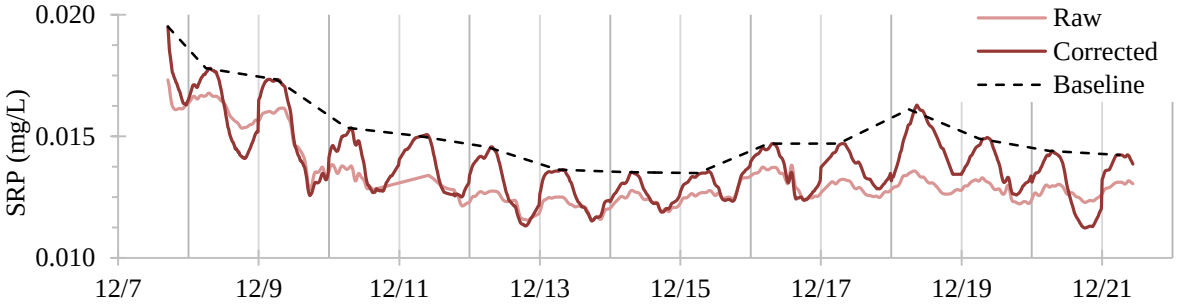

Figure 3-3. Raw (gray) and adjusted (black) PO4- signal with assimilatory baseline (dashed).

Average daily estimates of GPP, ER, U_{A-N} and U_{A-P} are provided in the table below. Regressions of GPP, U_{A-N} and U_{A-P} for all days within the deployments are shown in the figures.

Table 3-2 Summary of average values

Parameter	US	DS	Units
GPP	9.4	11.7	g-O_2/m^2/d
ER	13.7	16.3	g-O_2/m^2/d
U_{A-N}	92	127	mg-N/m^2/d
U_{D-N}	314	179	mg-N/m^2/d
U_{A-P}	7.2	17.0	mg-P/m^2/d
P:R	0.69	0.73	
C:N	24	22	
C:P	685	392	
N:P	28	19	

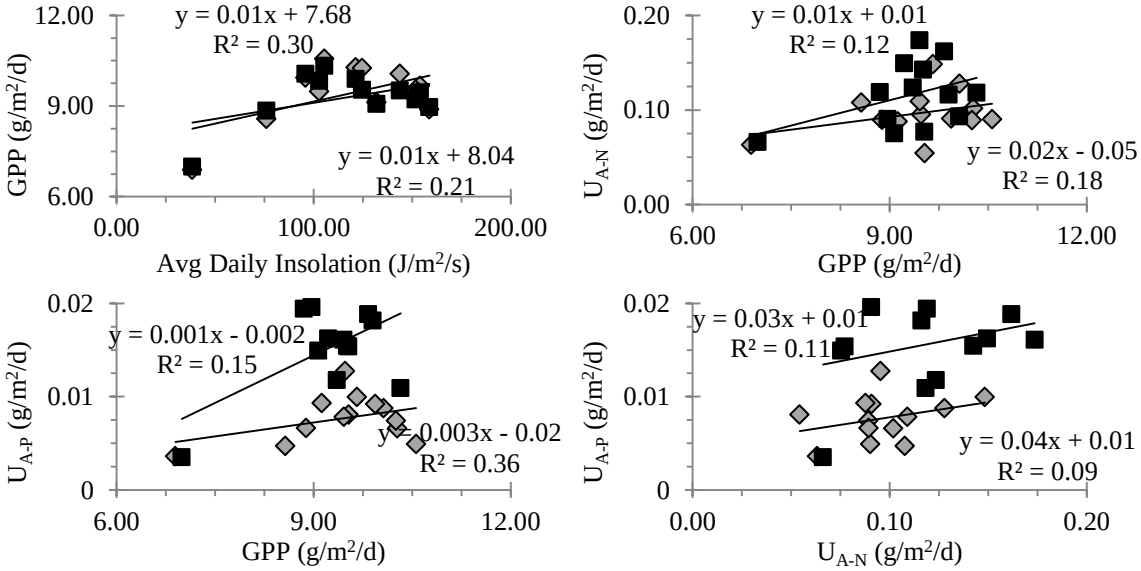

Figure 3-5. GPP vs. average daily insolation (top left) U_{A-N} vs. GPP (top right), U_{A-P} vs. GPP (top right) and U_{A-P} vs. U_{A-N} (bottom) for upstream (gray) and downstream (black) for each day of the deployment. Upstream regression equations are top left, downstream are bottom right.

Rates of daily GPP in both reaches were correlated with daily solar insolation (Figure 3-4). Estimates were markedly lower than those measured by Odum (1957), though consistent with more contemporaneous measurements (WSI 2010, Cohen et al. 2013b). Both reaches were net heterotrophic (P:R <1). This is consistent with the timing of the deployment in late December with reduced autochthanous production due to reduction in daylight hours and sun zenith angle, and greater allochthanous inputs of deciduous litterfall. The downstream reach has a higher P:R ratio than the upstream reach, while we would expect the opposite due to the accumulation of allochthanous material and a reduction in light transmittance due to reduced water clarity.

The daily Estimates of $U_{A\text{-}N}$ were found to be markedly consistent with those previously measured in Rainbow and other North Florida springs (Heffernan and Cohen 2010, Cohen et al. 2013, Hensley et al. 2014, Hensley et al. 2015, Hensley and Cohen 2016). Ecosystem C:N ratios were slightly lower in the downstream reach, consistent with lower tissue C:N in filamentous algal species, which are more prevalent in the lower reach. However in both reaches ecosystem C:N ratios were slightly higher than expected given tissue stoichiometry, a phenomenon observed in numerous other studies in spring rivers (Heffernan and Cohen 2010, Cohen et al. 2013, Hensley et al. 2014, Hensley et al. 2015, Hensley and Cohen 2016). This may suggest internal recycling of N (Sickman et al. 2009), uptake from a location other than the water column (i.e. roots), or assimilatory N derived from another N species. In Rainbow River we speculate that additional demand for assimilatory N, particularly in the downstream reach, may be met by NH_4^+ which is enriched in the lower Rainbow River. As NH_4^+ is a more preferable source of assimilatory N, it is likely that assimilatory demand in the downstream reach is being met by NH_4^+ rather than NO_3^-, and thus inflating the inferred C:N from NO_3^- profiles only. Currently sensors for capturing high resolution NH_4^+ profiles are not practically available although this may change in the near future.

The average daily estimate of $U_{A\text{-}P}$ was markedly higher in the downstream reach. This was not a result of correction for Ca^{2+} precipitation, as correcting the downstream signal would increase rather than decrease the inferred magnitude of $U_{A\text{-}P}$ in the downstream reach. It indicates a higher assimilatory demand for P in the downstream reach. While *Vaucheria* exhibits a higher C:P tissue stoichiometry, the dominant filamentous algal species in the lower Rainbow

River is *Lyngbya*, which does not exhibit a significantly different C:P ratio than vascular plant species. This additional demand may be from epiphytic or water column phytoplankton, which as single cell organisms likely have lower C:N:P ratios (e.g. Redfield 1958). We noted an increase in ChlA between the upstream and downstream stations (Figure 3-5).

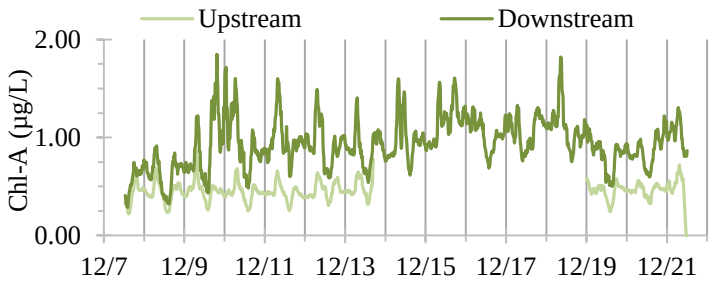

Figure 3-5 ChlA at upstream (gray) and downstream (black) stations.

A complete comparison of daily GPP, U_{A-N} and U_{A-P} between the upstream and downstream reaches for each individual day of the deployment is shown in the figure below. Dashed lines indicate trendlines with the intercept forced through zero. Daily variation in GPP was much more consistent across reaches versus U_{A-N}, which was in turn more consistent across reaches than U_{A-P}.

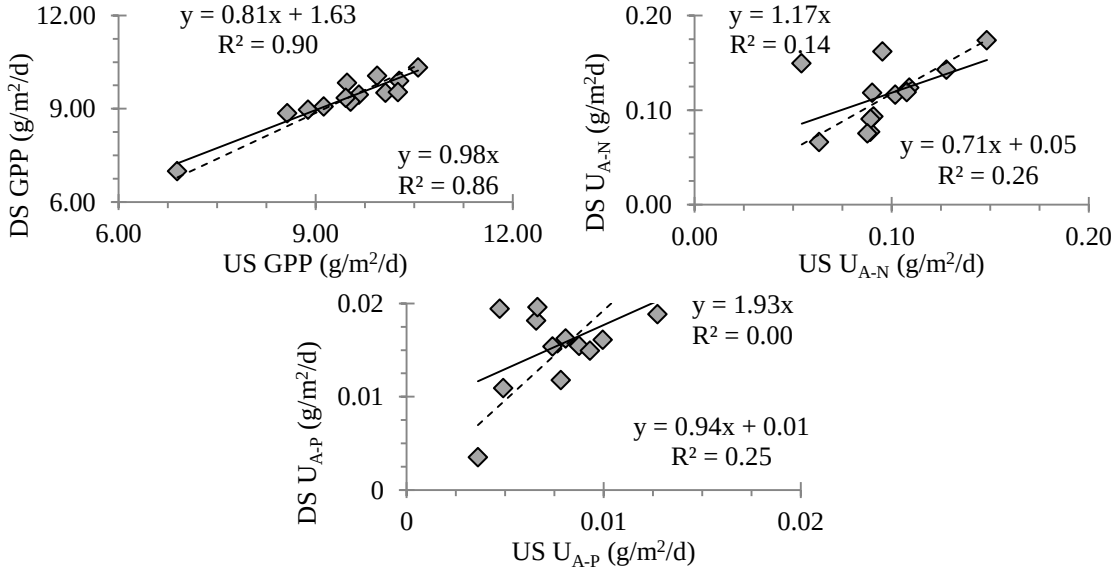

Figure 3-7. Downstream versus upstream daily estimates of GPP (top left), U_{A-N} (top right), and U_{A-P} (bottom) for each day of the deployment.

Finally, we examined U_{D-N}. This value represents the net dissimilatory removal of nitrate, and is equal to denitrification minus nitrification. Previous studies (Heffernan and Cohen

2010) have found this value to be correlated with the magnitude of the previous days GPP, as primary production produces the labile carbon which acts as the electron donor in denitrification. Here, we observed that $U_{D\text{-}N}$ does appear correlated with the previous days GPP in the upstream reach, but not in the downstream reach (Figure 3-7). This may be because in the upstream reach river water contained very little NH_3-N, while in the downstream reach it became substantial (see 2015 Annual Report). We speculate that in the upstream reach there is no appreciable nitrification, $U_{D\text{-}N}$ is almost entirely controlled by denitrification, and thus more closely coupled with GPP. In the downstream reach there is significant nitrification which counterbalances denitrification, the net value of $U_{D\text{-}N}$ is less (Table 3-2), and it is less closely coupled with GPP.

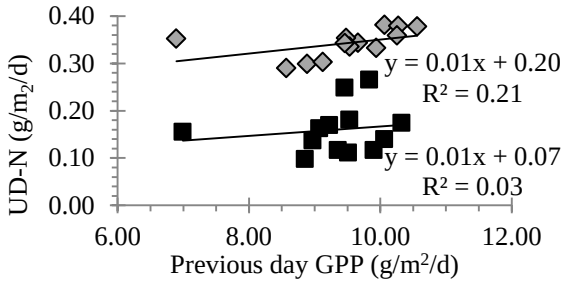

Figure 3-7. $U_{A\text{-}D}$ vs. previous day's GPP in upstream (gray) and downstream (black) reaches.

Longitudinal profiles exhibit substantial spatial variation. DO at the headsprings is 7.86 mg/L (Figure 3-8), below atmospheric saturation (ca. 9 mg/L), suggesting consumption of DO through vadose zone respiration during recharge and/or respiration within the aquifer. In the morning, DO generally declines with downstream distance, suggesting net heterotrophy (ER greater than GPP). In the afternoon, DO increases with downstream distance, even above the saturation concentration of ~9.00 mg/L, suggesting net autotrophy (GPP greater than ER). We note the decline in DO at the end of the afternoon profile is likely the result of the sampling craft catching back up to "older" water (See Hensley et al. 2014 for more on sampling artifacts in longitudinal profiles). Sampling vessel travel time was <2 hours while previous work (Hensley and Cohen 2012) suggests a mean residence time of ~12 hours. Water at the bottom of the river at 14:00 travelled only slightly longer in sunlight than darkness ($\Sigma GPP \approx \Sigma ER$), and thus has a concentration only slightly above saturation.

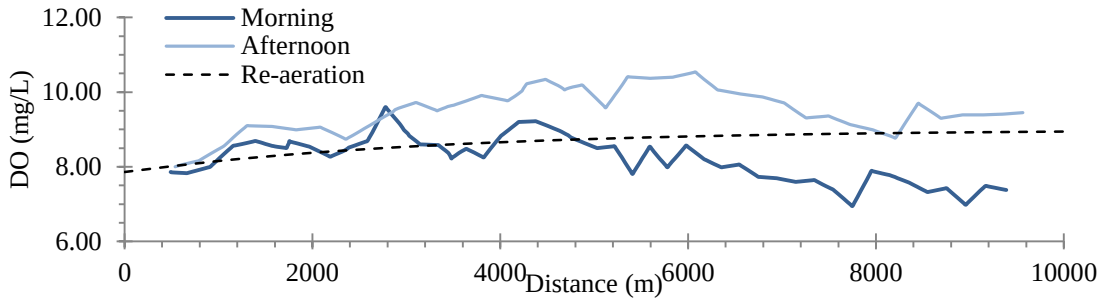

Figure 3-8. Longitudinal profiles of DO.

Assuming a k value of 5x10-5 s^{-1}, we calculated the expected profile based solely on re-equilibration with the atmosphere (dashed line Figure 3-8). ER was estimated from the slope of the difference between this line and the morning profile and was equal to 10.1 g-O_2/m_2/d. GPP was estimated from the slope of the difference between the afternoon profile and the morning profile and was equal to 11.1 g-O_2/m_2/d. Thus the river was slightly net autotrophic. As in the previous paragraph, we note that the morning profile was not a true nighttime profile and contains some influence of primary production. Thus the estimates of both ER and GPP are likely underestimates.

CO_2 at the headsprings is 2500-3000 ppm (Figure 3-9), substantially higher than atmospheric saturation (ca. 400 ppm), suggesting large amounts of respiration and production of CO_2 within the vadose zone and/or aquifer. Both profiles show initial declines in concentration with distance, likely the result of re-equilibration with the atmosphere. The afternoon profile declines more rapidly than the morning profile, and this additional removal of CO_2 can be inferred as the change in the balance of GPP:ER from morning to afternoon. We note that neither profile comes close to approaching atmospheric concentrations (~400 ppm), suggesting some additional process is adding CO_2 back to the water because GPP and aerobic ER should roughly be in balance over 24 hrs (i.e. day and night profiles should straddle dashed line). We speculate that this additional process is anaerobic respiration. We know anaerobic respiration processes which produce CO_2 must be happening (for example denitrification in subsequent paragraph), however these are the first direct measurements of CO_2 which show these processes to be potentially as large or larger than aerobic respiration. Thus ER estimates inferred from DO only may be gross underestimations of total respiration.

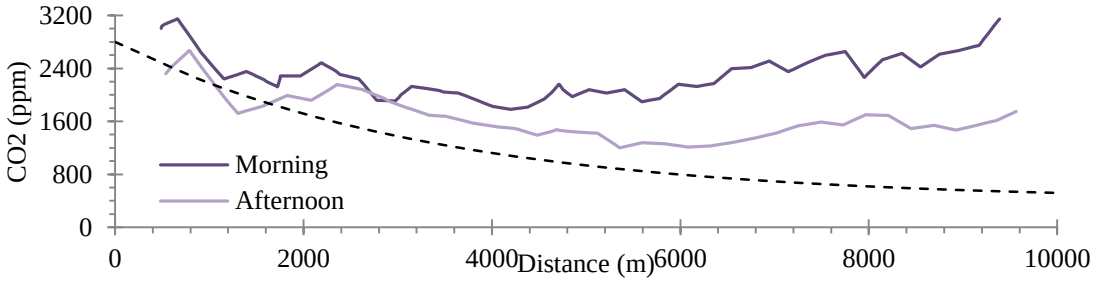

Figure 3-9. Longitudinal profiles of CO_2.

NO_3^- at the headsprings is 2.23 mg/L (Figure 3-10). The upper river exhibits initially rapid declines, however we believe this to largely be the result of dilution from additional inflow rather than biological processing. This is supported by previous work (Hensley et al. 2014) and the marked variability in the SpC profile in the first 2.5 km of the river observed during this set of profiles. Downstream of 2.5 km we note a gentler and steadier decline in NO_3^-, though still punctuated by abrupt changes at consistent locations, likely the location of additional springs. The afternoon profile shows a slightly greater decline, consistent with greater autotrophic assimilation of NO_3^-.

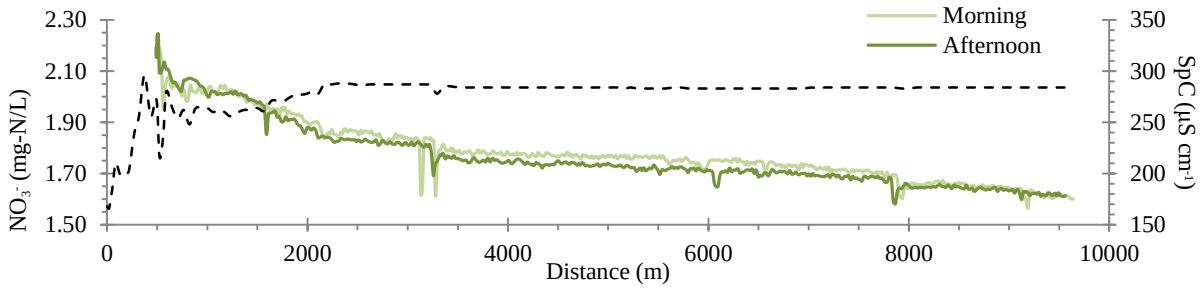

Figure 3-10. Longitudinal profiles of NO_3^- (solid lines) and SpC (dashed line).

The reach between the spring inputs near KP Hole (ca. 3.3 km) and the un-named spring input ca. 6 km, we can calculate NO_3^- uptake rates using the profile slope (Hensley et al. 2014). For the morning profile this rate was 703 mg-N/m^2/d and for the afternoon profile this rate was 788 mg-N/m^2/d. If we assume the morning profile contains minimal assimilatory uptake (see previous paragraphs) this value would correspond to the rate of dissimilatory uptake (U_D). If we further assume that this rate remains constant, the difference between the profiles would correspond to the rate of assimilatory uptake (U_A) and was equal to 85 g-N/m^2/d.

Using the estimated values of GPP and U_A (Table 3-3) we can calculate an autotrophic ecosystem C:N ratio of 29. This value is only slightly higher than the values obtained using the diel method in the previous section.

Table 3-3 Summary of average values

Parameter	Morning	Afternoon	Units
GPP	-	11.19	$g\text{-}O_2/m^2/d$
ER	10.11	10.11*	$g\text{-}O_2/m^2/d$
$U_{T\text{-}N}$	703	788	$mg\text{-}N/m^2/d$
$U_{D\text{-}N}$	703	703*	$mg\text{-}N/m^2/d$
$U_{A\text{-}N}$	-	85	$mg\text{-}N/m^2/d$
C:N		29	

* indicates values assumed from morning profile

The results of both the Eulerian and Lagrangian sampling suggest that assimilatory uptake of nutrients is strongly coupled with rates of primary productivity, which is in turn strongly correlated with solar insolation. This is consistent with the findings of Odum more than half a century ago (Odum 1957a and 1957b). Autotrophic demand for N was found to be around 100 $mg\text{-}N/m^2/d$, consistent with previous studies (Heffernan and Cohen 2010, Cohen et al. 2013, Hensley et al. 2014). Multiplying this by the benthic surface area of Rainbow River (average width 55m and length 9.5 km) results in an estimated total daily demand for autotrophic N of around 52 kg/day which seems like a large value. However multiplying average head spring concentration of 2.10 mg-N/L by average flow of 18,000 L/s results in an average daily supply of 3,266 kg/day. Thus supply of NO_3-N exceeds autotrophic demand for N by almost 2 orders of magnitude. Even at historic concentrations prior to anthropogenic enrichment of 0.08 mg-N/L (Odum 1957b), daily supply was 124 kg/day, or 250% demand (and this is conservative as it neglects that flows were historically higher). Thus is appears very hard to rationalize how NO_3^- concentrations could be controlling primary productivity. This is of course is not to say that the magnitude of primary production, or the composition of the autotroph community has not changed, just that NO_3^- concentrations have always been sufficient to meet any plausible level of autotrophic N demand. Increases over historic levels result in greater downstream export, and likely greater denitrification, but not increased primary production.

Section 4. Benthic Chamber Nutrient Amendments

Part 4.1 Nutrient Limitation of GPP

Methods

Benthic chambers have been extensively utilized to measure rates of stream metabolism (Hansmann et al. 1971, Bott et al. 1978, Bott et al. 1985). We constructed four identical chambers from transparent lexan polycarbonate. Dimensions were 60cm x 60cm x 120cm. The four chambers were deployed adjacent to each other, with the bottom inserted approximately 20 cm into the sediments and the top exposed to the atmosphere (Figure 4-1). This isolated an approximately 0.3-0.4 m^3 volume of water within each chamber. Each chamber contained a small electric aquarium pump to gently recirculate water and minimize stratification. For chambers placed where SAV was present, we estimated biomass by counting the total number of stems, measuring an average length and width, and multiplying by 1 g/cm^2 of leaf area (empirically derived from subsampling).

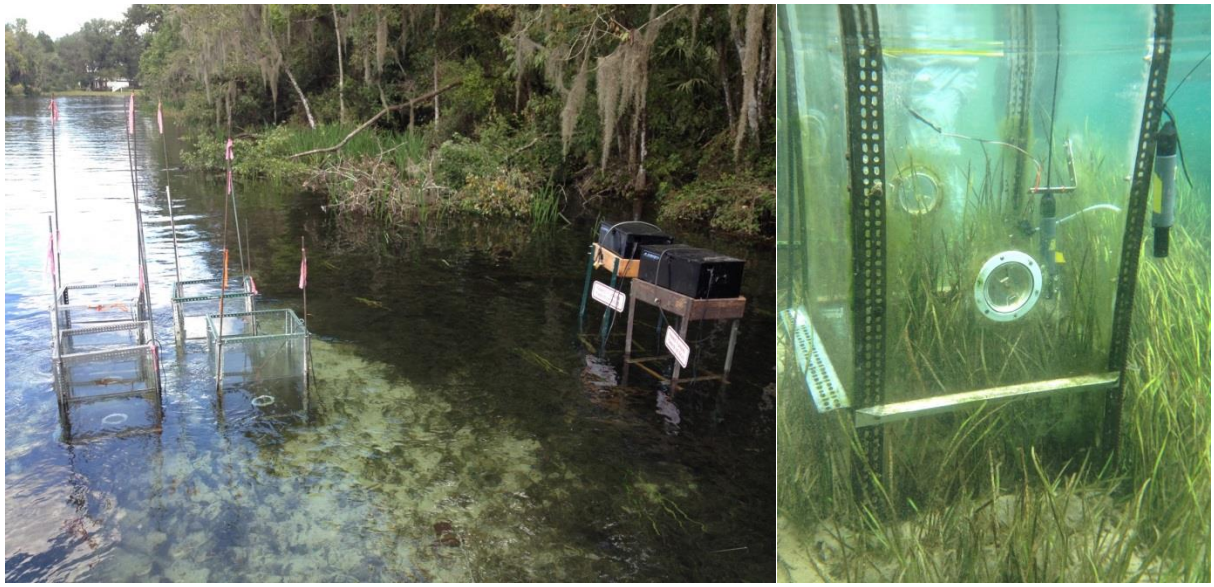

Figure 4-1. Set of four benthic chambers deployed in Rainbow River (left). Boxes in right of figure house batteries for pumps and sensors. Underwater view (right) showing HOBO sensors deployed inside and outside of chamber.

Within the cluster of four benthic chambers, one chamber served as a control, while the other three received a unique nutrient treatment comprised of N, P, Fe, N+P, N+Fe, P+Fe, N+P+Fe. NO_3^- or PO_4^- were enriched five-fold over ambient concentrations, while Fe^{2+} treatments were enriched ten-fold. NaCl was added to each box as a conservative tracer to ensure no leaking. After addition, sufficient time was allowed for complete mixing, and then a pre-deployment sample was collected from each box.

Above each chamber, a pendent light meter (Onset, Bourne MA) measured light at 15 minute intervals. Within each chamber was a HOBO DO sensor (Onset, Bourne MA) which was programed to sample at 15 minute intervals (Figure 4-1). The rate of change in DO was used to calculate gross primary production (GPP) and ecosystem respiration (ER). The effect of DO re-aeration was estimated based on findings using a propane injection and adjusted for DO based on the molar masses (Reijo et al. in review). ER was calculated as the average nighttime change in DO after correcting for re-aeration. GPP was calculated as the daytime increase over the value of ER. For a more detailed explanation of this method see Odum 1956 and 1957.

To measure epiphytic algal growth as an additional metric to quantify nutrient enrichment response, we suspended an 11x11 cm square unglazed ceramic tile in each chamber. Algal biomass was determined by scraping the tiles and collecting the biomass into a DI solution; this solution was passed through a pre-weighed 0.45 μm glass fiber filter. The filter disk was then dried at 75°C for 24 hours and re-weighed to determine the algal biomass.

We recorded GPP and epiphytic algal growth in each box over a period of one week. At the end of each week, post-deployment samples were collected from each chamber. The chambers were then scrubbed free of any accumulated algae and repositioned as a cluster in a new location within the river. Site locations were selected to include bare, algal, and SAV dominated substrate. In total, 3 replicates of 7 nutrient combinations were performed on 3 substrate types, for a total of 63 replicates or 21 deployments (1 control + 3 treatment per deployment). Note the actual number ended up being more because Cl^- analysis suggested some boxes leaked and had to be re-performed. Data collection was started in July 2015 and completed in May 2016.

Results: Control Chambers

All chambers exhibited diel variation in DO indicative of primary production. Within just the control chambers, substantial variation was observed across deployments (Figure 4-2). Observed DO concentrations varied from 1.34 to 23.45 mg/L. Supersaturation of DO was possible due to reduced turbulence and therefore reduced gas exchange in the benthic box compared to the river. Weekly average GPP across deployments varied from 2.14 to 19.71 g-O_2 m^2/d with an overall mean of 7.91 g-O_2 m^2/d.

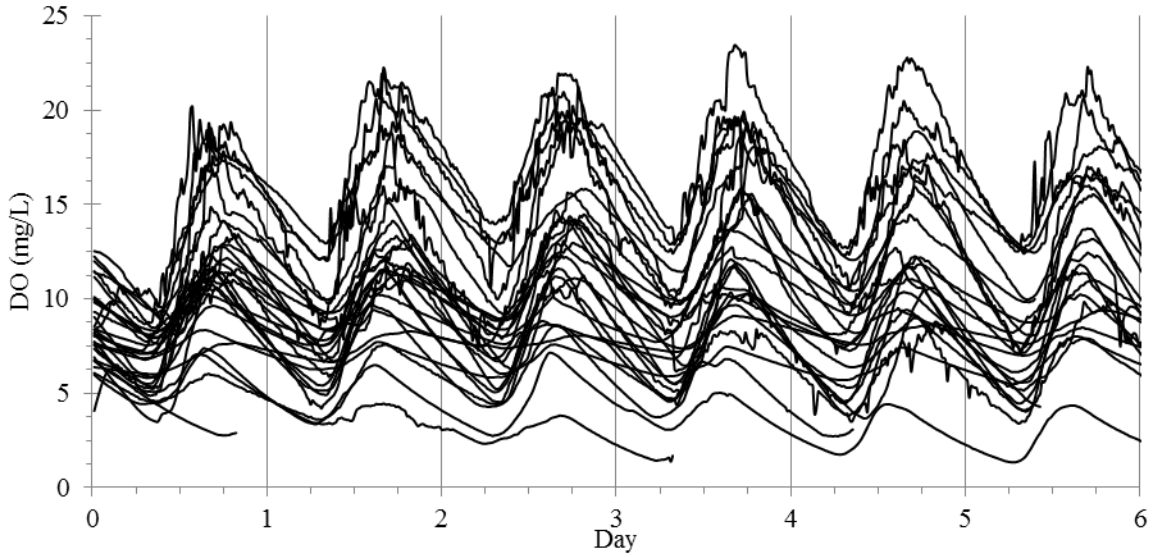

Figure 4-2 Control chamber dissolved oxygen profiles.

To determine whether chamber artifacts might influence rates of GPP over the course of deployments (for example accumulation of algae obstructing light, or the depletion of nutrients) for each deployment we regressed daily GPP versus deployment day. A positive slope indicated increasing daily GPP over the course of the deployment while a negative slope indicated decreasing daily GPP over the deployment. Across all deployments we observed slopes to be normally distributed with a mean only slightly larger than zero (Figure 4-3). This finding suggests there is likely not a cumulative chamber effect on GPP.

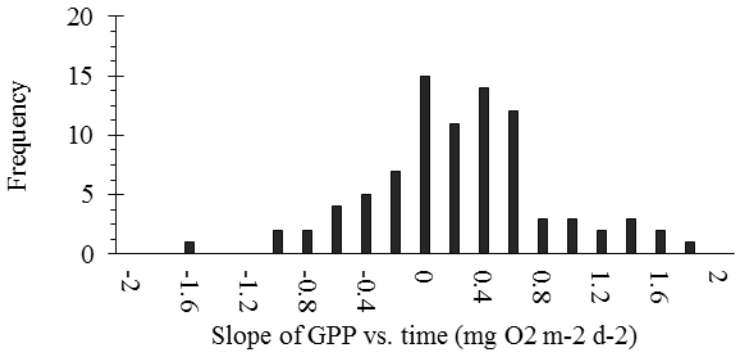

Figure 4-3 Distribution of slopes of GPP vs. time

To determine the factors that affect GPP variation across the control boxes, we developed a general linear model with light, season, downstream distance, cover type (SAV, filamentous algae or bare), and depth as predictors. The best fit model explained 70.6% of the variation in control box GPP. The model contained an interaction between cover and light (Table 4-1). Follow up, pairwise comparisons showed that GPP varied strongly according to cover type (p=<0.001), with bare areas only 57% as productive as those areas comprised of filamentous algae or rooted macrophytes, which were nearly the same (Figure 4-4). Light explained 45% of the variance in the control boxes (p=<0.001) (Figure 4-4). Nitrogen (p=0.657), phosphorus (p=0.993), depth (p=0.224), and river distance (p=0.682) from headspring were not significant predictors of control-box GPP.

Table 4-1. General linear model of control chamber GPP

	Estimate	Std. Error	t value	p
(Intercept)	-3.395	2.2172	-1.531	0.140
Light	**0.056**	**0.010**	**5.449**	**<0.001**
Bare	4.342	3.269	1.328	0.198
SAV	6.094	6.79946	0.896	0.380
Light:Bare	**-0.031**	**0.016**	**-1.911**	**0.069**
Light:SAV	-0.019	0.036	-0.534	0.599
Residual Deviance			98 on 21 degrees of freedom	
Null Deviance			333 on 26 degrees of freedom	

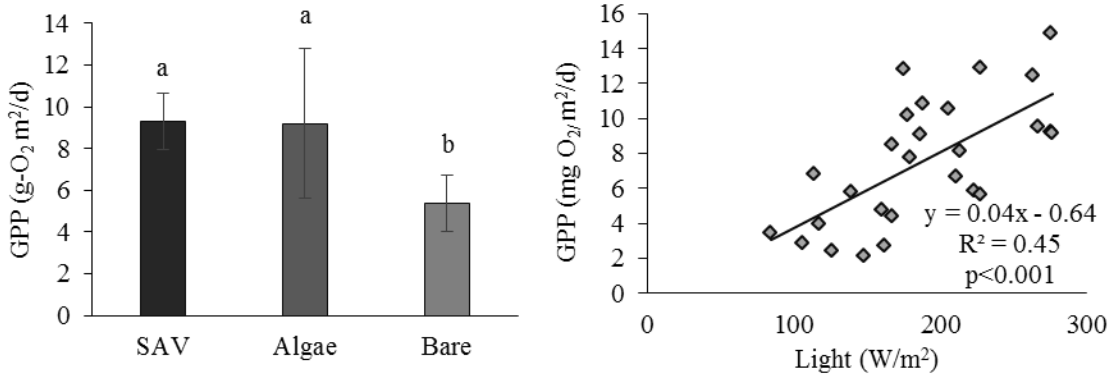

Figure 4-4. Vegetated versus bare benthic cover (left) and light (right) were significant predictors of GPP.

Results: Nutrient Enrichment Assay Chambers

To assess the GPP response to nutrient additions despite temporal variation in sunlight, we used a response ratio, with GPP in each treatment box compared to GPP in a commensurate control box over each week-long deployment. That is, the response ratio (RR_{GPP}) is defined as $GPP_{treatment}/GPP_{control}$. Where a nutrient addition treatment increased primary production, this value will exceed 1, and values below 1 indicate an inhibitory response. Because of the asymmetry in the effect magnitude between stimulatory and inhibitory effects, we take the $\log_{10}$ of this response ratio. As such, positive values of the $Log_{10}RR_{GPP}$ indicate a stimulatory response, while negative values indicate an inhibitory response. We follow the same logic for biomass-indexed GPP (GPP_{bio}) and for epiphytic algal biomass accumulation on growth tiles (ALG).

We first considered the GPP response only, comparing mean values of $Log_{10}RR_{GPP}$ across the 7 nutrient addition treatments (N, P, Fe, N+P, N+Fe, P+Fe, N+P+Fe). We note that despite deploying 63 treatment boxes across 21 deployments, we obtain relatively low power to detect nutrient enrichment effects given the intrinsic heterogeneity that exists in benthic cover at the box-footprint scale. Moreover, our deployments are distributed evenly across 3 benthic cover types (SAV dominated, filamentous algal dominated, bare). The best model using the factorial experimental design, intended to capture nutrient addition interactions, suggested no cover type effect, and a weak ($p = 0.06$) stimulatory effect of Fe added alone and along with P (Fig. 4-6, Table 4-2). Both effects were small in magnitude (increasing GPP by ~15%), but potentially biologically significant. Notably, there was no significant effect of Fe added with N,

or when all three nutrients were added together. This model explained approximately 20% of the variation in the GPP response; using the AIC score, we determined that the inclusion of additional variables (e.g., water depth, light, season) was not warranted.

Table 4-2. Summary of general linear model of GPP response to factorial nutrient treatments.

```
Coefficients:  Estimate       Std. Error     t value        Pr(>|t|)
N + P + Fe     0.04384        0.03341        1.312          0.1951
Fe             0.06298        0.03341        1.885          0.0649 .
N              0.04216        0.03789        1.113          0.2708
N + Fe         0.04036        0.03341        1.208          0.2324
N + P          -0.01533       0.03341        -0.459         0.6482
P              -0.03233       0.03341        -0.967         0.3377
P + Fe         0.06806        0.03471        1.961          0.0502 .
---
Signif. codes:  0 ‘***’ 0.001 ‘**’ 0.01 ‘*’ 0.05 ‘.’ 0.1 ‘ ’ 1
    Null deviance: 0.6612  on 60  degrees of freedom
Residual deviance: 0.5325  on 53  degrees of freedom
AIC: -97.196
```

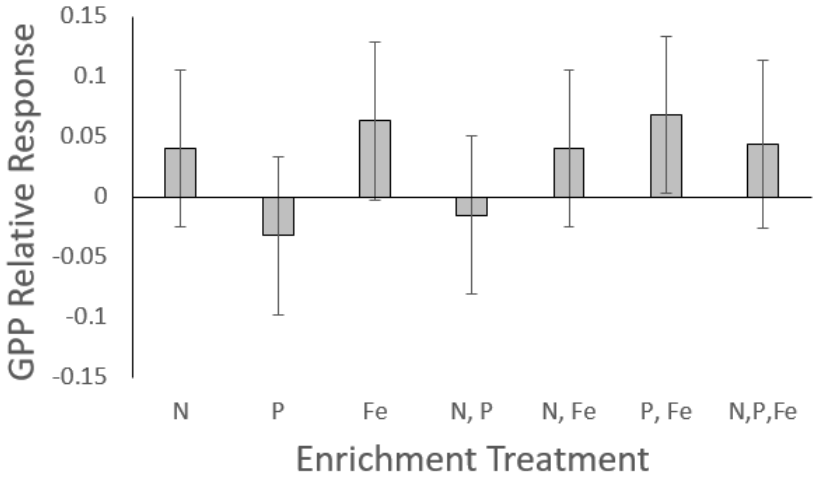

Fig. 4-6 – Treatment means for $Log_{10}RR_{GPP}$, pooled across benthic cover type (for which no significant effect was observed). Values > 0 indicate a stimulatory effect of a treatment, while values < 0 indicate an inhibitory effect. Error bars are 95% confidence intervals.

By further exploring the individual effects of nutrient additions, we were able to identify whether the weak Fe impact on GPP was robust. To that end, we explored how N, P, and Fe additions impacted the GPP response ratio, regardless of whether each solute was added alone or in combination. This binary comparison revealed a slightly improved model (given the AIC scores) but a similar result, with a marginally significant stimulatory effect of Fe additions, and no effect of either N or P (Table 4-3, Fig. 4-6). The fitted slope further supported that the average magnitude of the stimulatory effect was around 15% of control box GPP, which may be biologically significant. Further exploration of the Fe effect across benthic cover types (Fig. 4-8, Table 4-4) suggested that the growth stimulation was positive for all sites, regardless of cover

(bare, SAV, and filamentous algal dominated). However, the effect was only significant (p = 0.01) and largest (slope = 0.078) for filamentous algal sites, suggesting nearly 20% increase in GPP for filamentous algal dominated settings, roughly double the effect in SAV and bare settings.

Table 4-3. Results of general linear model of RR_{GPP}

```
glm(formula = LogGPPRR ~ fe + n + p, data = final.box.data)

Coefficients:  Estimate       Std. Error     t value        Pr(>|t|)
(Intercept)    0.010936       0.032148       0.320          0.7504
fe             0.053514       0.027143       1.972          0.054 .
n              -0.00071       0.026465       -0.027         0.9785
p              -0.021985      0.025506       -0.810         0.4214
---
Signif. codes:  0 ‘***’ 0.001 ‘**’ 0.01 ‘*’ 0.05 ‘.’ 0.1 ‘ ’ 1

    Null deviance: 0.61101  on 59  degrees of freedom
Residual deviance: 0.55406  on 56  degrees of freedom
AIC: -100.82
```

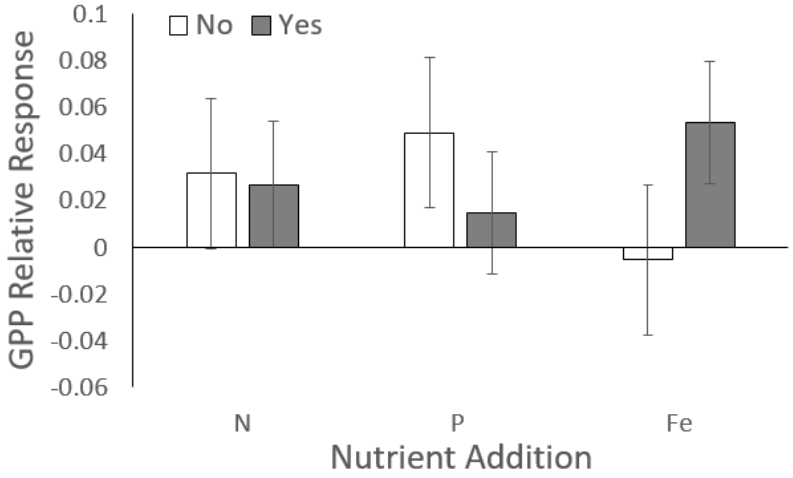

Fig. 4-7 – Response ratios for binary nutrient additions. The mean with and without solute additions were compared, and Fe exhibited a modest significant stimulatory effect (p = 0.06).

Table 4-4. Results of Fe enrichment on the GPP relative response across cover types.

```
glm(formula = LogGPPRR ~ fe:cover - 1, data = final.box.data.v2)

Coefficients:  Estimate       Std. Error     t value        Pr(>|t|)
Fe:Algae       0.07828        0.03114        2.514          0.0148 *
Fe:Bare        0.04103        0.02731        1.503          0.1385
Fe:SAV         0.04608        0.02842        1.621          0.1105
---
Signif. codes:  0 ‘***’ 0.001 ‘**’ 0.01 ‘*’ 0.05 ‘.’ 0.1 ‘ ’ 1

    Null deviance: 0.66120  on 60  degrees of freedom
Residual deviance: 0.55255  on 57  degrees of freedom
AIC: -102.98
```

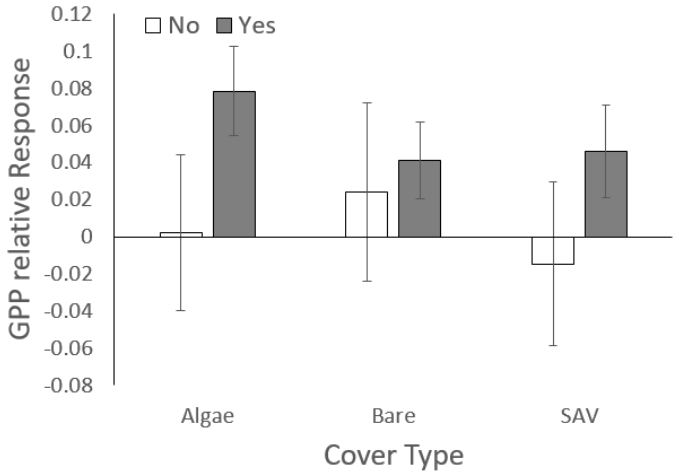

Fig. 4-8 – Response ratios for Fe additions across cover types. While Fe additions always had a positive effect on the GPP response ratio, it was significant (p = 0.01) only for algal sites.

Finally, we note that when the effects of P enrichment were evaluated as a function of cover, we observed a significant inhibitory effect (p = 0.03) in SAV-dominated sites. No similar effect was present for bare and filamentous algal dominated sites. The magnitude of the effect (Table 4-5) suggests that added P reduced SAV GPP by roughly 20%, a finding that, if persistent and confirmed, could be a of considerable significance in Rainbow River, where P availability so dramatically varies long the river length.

Table 4-5. Results of P enrichment on the GPP relative response across cover types.

```
glm(formula = LogGPPRR ~ p:cover, data = final.box.data.v2)

Coefficients:  Estimate       Std. Error     t value        Pr(>|t|)
(Intercept)    0.049008       0.019849       2.469          0.0166 *
P:Algae        0.004612       0.035908       0.128          0.8983
P:Bare         -0.025173      0.034853       -0.722         0.4731
P:SAV          -0.079482      0.034853       -2.280         0.0264 *
---
Signif. codes:  0 ‘***’ 0.001 ‘**’ 0.01 ‘*’ 0.05 ‘.’ 0.1 ‘ ’ 1

    Null deviance: 0.61101  on 59  degrees of freedom
Residual deviance: 0.55156  on 56  degrees of freedom
AIC: -101.09
```

These results suggest a potentially important role of Fe in regulating metabolism in Rainbow River, and point further to the magnitude of that effect being greatest under conditions with high algal biomass. While these should be viewed as tentative inferences, particularly since the evidence for statistically significant effects is marginal, further exploration of the sources, controls, and fate of Fe appear to be warranted.

Nutrient enrichment effects based on GPP only are somewhat challenging to detect because of considerable extant variation in benthic biomass. Primary production is a mass specific process; that is, more biomass can maintain higher rates of productivity. Despite our efforts to select sites with homogeneous benthic biomass (e.g., by selecting apparently uniform SAV meadows or algal mats), post-deployment investigation revealed that biomass standing stocks could vary between adjacent boxes considerably. To remedy this problem, we further normalizes control versus treatment chamber GPP (i.e., GPP:biomass) using the measured biomass within each chamber for the SAV sites (n = 20 deployments). This enabled a second response ratio ($RR_{GPP,B}$) that is the normalized GPP:biomass in the treatment box divided by the normalized GPP in the control box. As before, we take the log of the ratio to ensure symmetry of stimulatory and inhibitory effects. That is, $Log_{10}RR_{GP,B} = Log\ (GPP_{B,treatment}:GPP_{B,control})$, where GPP_B refers to GPP normalized to biomass standing stocks.

This analysis also revealed a significant stimulatory effect of Fe additions, alone and in combination with P and with N and P (though, notably, N + Fe was not significant) (Table 4-6 and Figure 4-9). The magnitude of the stimulatory effect was larger than previously, indicating GPP stimulation of biomass-indexed GPP by as much as 60%, though we note that these estimates are uncertain, having been derived from 3 replicates of each treatment. Overall, the model explained 58% of the observed variation in the response ratio, which was a marked improvement over the model for $Log_{10}RR_{GPP}$ implemented across cover types. While we explored conditioning the model response further based on mean GPP, water depth, and light, AIC scores suggested that including these variables was not justified.

Table 4-6. Summary of general linear model of the GPP_B Response Ratio given factorial nutrient treatments. Subscript B indicates that response has been normalized by SAV biomass.

```
glm(formula = LogGPPBRR ~ treat - 1, data = final.box.data.v2)

Coefficients:  Estimate       Std. Error     t value        Pr(>|t|)
N + P + Fe     0.228145       0.085392       2.672          0.0182 *
Fe             0.213773       0.085392       2.503          0.0253 *
N              0.024695       0.085392       0.289          0.7767
N + Fe         0.006770       0.085392       0.079          0.9379
N + P          0.068737       0.085392       0.805          0.4343
P              -0.002318      0.085392       -0.027         0.9787
P + Fe         0.203559       0.085392       2.384          0.0318 *
---
Signif. codes:  0 ‘***’ 0.001 ‘**’ 0.01 ‘*’ 0.05 ‘.’ 0.1 ‘ ’ 1

    Null deviance: 0.73997  on 21  degrees of freedom
Residual deviance: 0.30625  on 14  degrees of freedom

AIC: -13.19
```

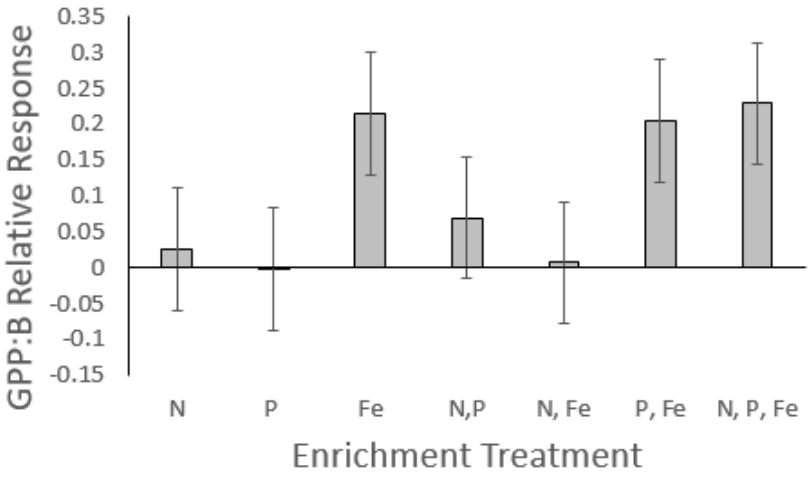

Fig. 4-9 – Treatment means for $Log_{10}RR_{GPP,B}$. These are for SAV sites only, where standing stock biomass estimates were available. Values > 0 indicate a stimulatory effect of a treatment, while values < 0 indicate an inhibitory effect. Error bars are 95% confidence intervals.

As before, we observed support for Fe stimulation of GPP when we considered individual nutrient enrichment effects, regardless of whether the solute was added alone or in combination. That is, the $Log_{10}RR_{GPP,B}$ was evaluated in response to N, P and Fe additions, which revealed a significant but weaker Fe effect (Table 4-7, Fig. 4-10), suggesting a roughly 40% stimulation of GPP, and no P or N effect. As before, addition of light, depth, and mean GPP did not improve model performance, which was able to explain 47% of the observed variation. We further note that, unlike the raw GPP response ratio, there was no evidence of a P inhibition effect of GPP_B.

Table 4-7. Summary of general linear model of the GPP_B Response Ratio given individual nutrient treatments. Subscript B indicates that response has been normalized by SAV biomass.

```
glm(formula = LogGPPBRR ~ (n + p + fe) - 1, data = final.box.data.v2)

Coefficients:  Estimate       Std. Error     t value        Pr(>|t|)
N              -0.02067       0.05190        -0.398         0.695
P              0.06422        0.05190        1.237          0.232
Fe             0.14128        0.05190        2.722          0.014 *
---
Signif. codes:  0 ‘***’ 0.001 ‘**’ 0.01 ‘*’ 0.05 ‘.’ 0.1 ‘ ’ 1

    Null deviance: 0.73997  on 21  degrees of freedom
Residual deviance: 0.38790  on 18  degrees of freedom
  (41 observations deleted due to missingness)
AIC: -16.227

Number of Fisher Scoring iterations: 2
```

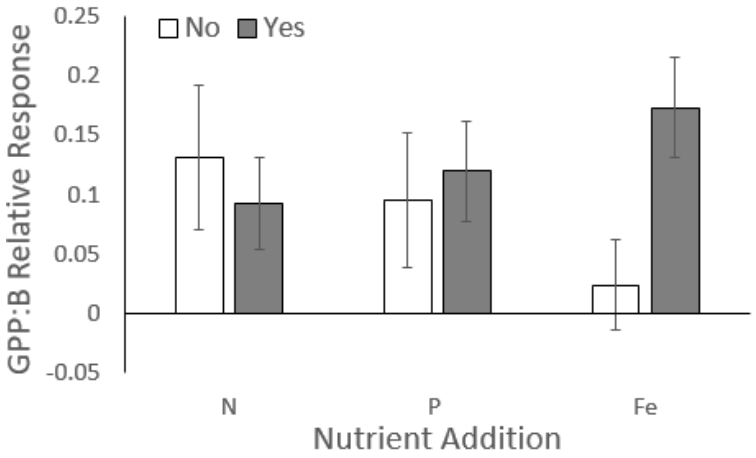

Fig. 4-10 – Nutrient enrichment means for $Log_{10}RR_{GPP,B}$. These are for SAV sites only, where standing stock biomass estimates were available. Values > 0 indicate a stimulatory effect of a solute enrichment regardless of whether that enrichment was alone or in combination with another solute. Values < 0 indicate GPP_B inhibition. Error bars are 95% confidence intervals.

In addition to GPP, we can explore the impact of nutrient enrichment on epiphytic algal accumulation on ceramic tiles suspended in select boxes. Epiphytic algal accumulation on tiles deployed in each box varied from 0.03 to 1 $g/m^2/d$, and this dramatic variation again necessitated considering the response relative to the control box in each week-long deployment. That is, the algal response ratio (RR_{algae}) is defined as the epiphytic algal biomass (ALG) on the tile in the treatment box ($ALG_{treatment}$) divided by the epiphytic algal biomass on the time in control box ($ALG_{control}$). The log_{10} of the relative response was obtained to make stimulatory and inhibitory effects symmetrical. Values of $Log_{10}RR_{algae}$ that are positive indicate a stimulatory effect of a nutrient enrichment treatment, while negative values indicate an inhibitory effect.

As before, we initially evaluated the impact of the factorial nutrient addition treatments, noting that algal tile data were only available for 26 replicates. The resulting general linear model (Table 4-8) explains 40% of the algal tile relative response, and suggests a significant effect of all three nutrients added together, and a marginal effect of P and Fe added together (Fig. 4-12).

Table 4-8. Summary of general linear model of the relative response of algal tile biomass accrual given the factorial nutrient treatments.

```
glm(formula = logTileRR ~ treat - 1, data = final.box.data.v2)

Coefficients:  Estimate      Std. Error     t value        Pr(>|t|)
N + P + Fe     0.576253      0.229632       2.509          0.0213 *
Fe             0.082701      0.093747       0.882          0.3887
N              -0.004092     0.162374       -0.025         0.9802
```

```
N + Fe          0.050594       0.102695       0.493          0.6279
N + P           -0.072438      0.102695       -0.705         0.4891
P               0.110846       0.132578       0.836          0.4135
P + Fe          0.223868       0.114816       1.950          0.0661 .
---
Signif. codes:  0 ‘***’ 0.001 ‘**’ 0.01 ‘*’ 0.05 ‘.’ 0.1 ‘ ’ 1

    Null deviance: 1.6514  on 26  degrees of freedom
Residual deviance: 1.0019  on 19  degrees of freedom
  (34 observations deleted due to missingness)
AIC: 5.1233
```

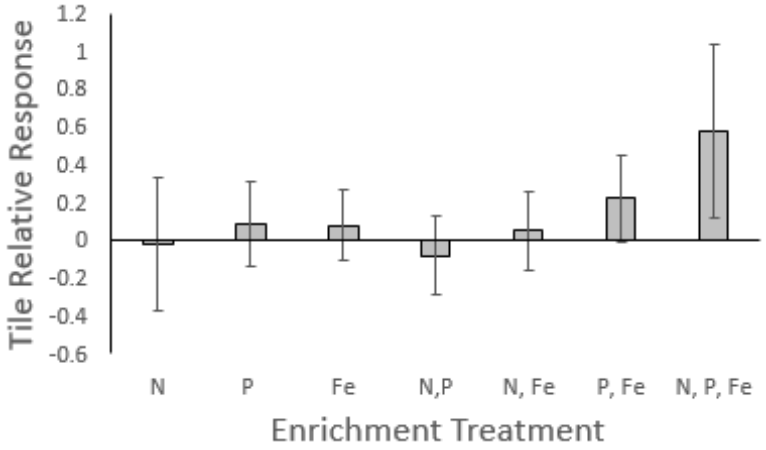

Fig. 4-11 – Treatment means for $Log_{10}RR_{ALG}$. These are for algal biomass accrual on tiles deployed in each treatment and control box. Values > 0 indicate a stimulatory effect of a treatment, while values < 0 indicate an inhibitory effect. Error bars are 95% confidence intervals.

Notably, none of the single nutrient additions were significant, and the effect magnitudes were confusing, with an implausibly large effect (ca. 325% stimulation) of the N + P + Fe, and a large effect (>60% stimulation) of P + Fe, but with no commensurate single nutrient effects; we note that these effects were generally based on 3 replicates. In short, the small sample size and large uncertainties inspire little confidence in the conclusions. To further explore the data, and obviate the low sample sizes created by distributing replicates across 7 factorial nutrient addition treatments, we further considered the nutrient enrichment effects regardless of whether they were added alone or in combination with others. These results convey a result more consistent with other results obtained here, with a significant Fe effect (p = 0.05, Table 4-9, Fig. 4-12) on the order of a 40% stimulation of epiphytic algal biomass accrual vis-à-vis the control, and no significant N or P effect. This model explained roughly 25% of the observed variation in epiphytic algal growth, so clearly failed to capture key factors. We further noted, when adding ancillary controls such as light, depth, and mean GPP, that water depth was an important model covariate. Adding depth, the fitted slope of which implied that epiphytic algal response was

greater in deeper water, allowed the model to explain 33% of the observed variation. The fitted slope for Fe suggests a relatively strong stimulatory effect (nearly 80% stimulation of epiphytic algal accrual), so while large uncertainties limit statistical significance to p = 0.03, the biological significance warrants attention. As with GPP_B we observed no significant P inhibition effect, as was observed for GPP.

Table 4-9. Summary of general linear model of the Algal Biomass Response Ratio given individual nutrient treatments.

```
glm(formula = logTileRR ~ (n + p + fe) + depth, data = final.box.data.v2)

Coefficients:  Estimate       Std. Error     t value        Pr(>|t|)
(Intercept)    -0.784416      0.320928       -2.444         0.0234 *
N              -0.009792      0.092509       -0.106         0.9167
P              0.166515       0.099845       1.668          0.1102
Fe             0.258963       0.109753       2.360          0.0281 *
Depth          0.008038       0.003459       2.324          0.0303 *
---
Signif. codes:  0 ‘***’ 0.001 ‘**’ 0.01 ‘*’ 0.05 ‘.’ 0.1 ‘ ’ 1

    Null deviance: 1.46809  on 25  degrees of freedom
Residual deviance: 0.94055  on 21  degrees of freedom
  (34 observations deleted due to missingness)
AIC: 0.29717
```

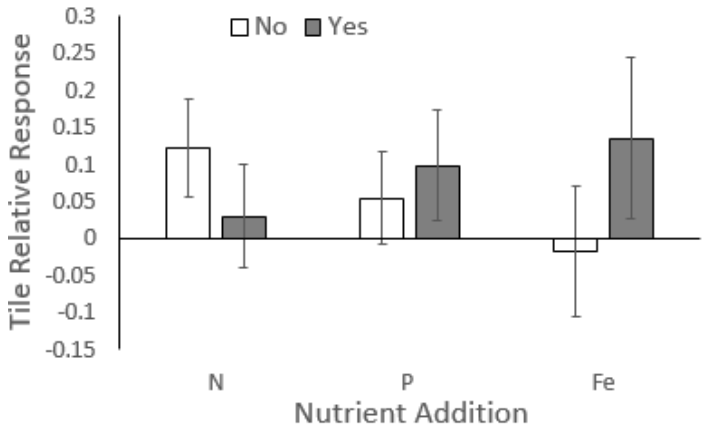

Fig. 4-12 – Nutrient enrichment means for $Log_{10}RR_{ALG}$, or the response of algal biomass accumulation on tiles in each chamber. Values > 0 indicate a stimulatory effect of a solute enrichment regardless of whether that enrichment was alone or in combination with another solute. Values < 0 indicate algal biomass inhibition. Error bars are 95% confidence intervals.

We note that epiphytic algal biomass accrual was strongly related to GPP (Fig. 4-13). Given this effect, we conclude that the stimulatory effect of any nutrient enrichment vis-à-vis the control is not confined to high GPP situations. In other words, while conditions that favor high GPP also favor epiphytic algal biomass accrual, the relative effect of nutrient enrichment, in our case confined nearly entirely to the stimulatory effects of Fe, is not predicated on site

productivity. This is surprising since we expect nutrient limitation is worst when demand is highest (e.g., under conditions of high GPP).

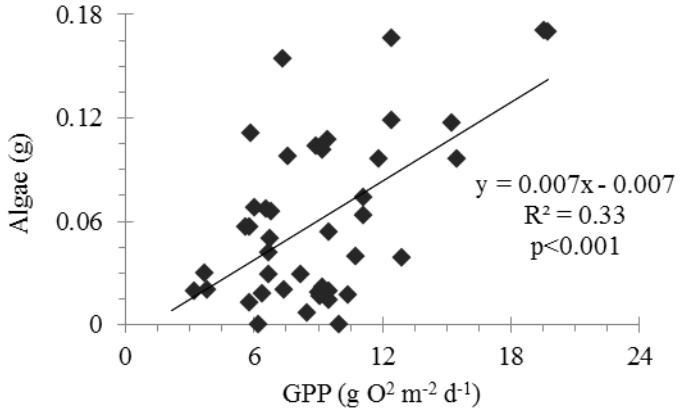

Figure 4-13 Algal growth versus GPP.

Primary production over time tends to increase (mean slope = +0.13) even though N concentration decreased markedly over the deployment period and P, on average, also decreased. Fe would presumably behave similarly, but was below analytical detection limits. This positive mean slope suggests that depletion of nutrients does not inhibit GPP and could be construed as evidence of weak or absent nutrient limitation. Increasing GPP could be a result of box design as phytoplankton could accumulate without constant flushing as well as increased epiphytic algae retention due to a loss in sloughing.

In summary, the benthic enrichment experiments suggest that gross primary production and epiphytic algal biomass accrual were similarly stimulated by Fe additions, and not by N or P additions. We also observed a significant reduction in GPP with P enrichment in boxes where vascular plants dominated; this was not observed for filamentous algal and bare substrates, and the effect was not evident when GPP was adjusted for biomass standing stock (i.e., GPP_B). In general, the degree of uncertainty associated with these inferences would encourage caution interpreting this result. However, the contention that P addition inhibits GPP for macrophyte chambers parallels what has been observed in some nutrient diffusing substrate studies (Johnson et al., 2009; Sanderson et al., 2009; Tank & Dodds, 2003). This may result from changes in microalgal community composition (e.g., elevated P disaggregating that biofilm), or even a toxicity effect on metabolism from high P concentrations. We note that if the effect was entirely due to macrophyte responses, we would have expected it to be evident when we considered

GPP_B not just GPP. While inference that P may inhibit SAV is tentative, at best, the particular situation in Rainbow River supports further attention to this hypothesis. There is a marked longitudinal gradient in P availability between the head spring and the Withlacoochee, with values increasing many-fold, and along which SAV cover declines precipitously. While there are clearly multiple factors at work, the potential impact of P enrichment, either in the water or the porewaters, merits consideration for explaining the observed patterns of SAV abundance in Rainbow River.

The consistent evidence for an Fe enrichment effect that stimulates both primary production and algal biomass is of potentially great management relevance. Fe has received relatively little attention as a control variable in springs. This work demonstrates that measurements of water column and pore-water Fe concentrations are exceedingly hard to measure because they are so low. Large amounts of iron are bound to the sediments, and this Fe mass increases with distance downstream (260 to 4576 mg/kg), corresponding with the increase in filamentous algae prevalence in Rainbow River (See Section 1). Fe may play a vital role in the competition between algae and vascular plants as tissue stoichiometry because algal demand for Fe per unit carbon (i.e., Fe:C) is an order of magnitude higher in algae than in rooted vascular plants (Kurz et al., 2013). In other words, an increase in Fe availability is likely to have a far greater stimulatory effect on algae than on SAV. A similar but smaller stoichiometric difference for N is the putative basis for the N enrichment hypothesis, whereby increased N availability enables faster growth by algal taxa that require more N per unit C. While the evidence for N effects on growth or biomass accrual are absent the logic for imputing nutrient limitation from tissue differences is still widely used. The combination of extremely low soluble Fe concentrations in general (i.e., conditions under which limitation should be expected), along with longitudinal trends in Fe availability, and finally coupled with order-of-magnitude differences in Fe:C ratios between the competing elements of the autotroph community lend support for the plausibility of Fe limitation in general. Moreover, high nitrate concentrations can induce Fe deficiency in aquatic plants by restricting availability by altering cell pH, thereby immobilizing Fe (Osborne et al., 2015; Smolders et al., 1997). As such, Fe limitation may be exacerbated in modern N-enriched waters.

Our results support a consistent and biologically relevant impact of Fe enrichment. For GPP, the magnitude of this effect is that the addition of Fe increases GPP by roughly 20%, and

principally in locations dominated by filamentous algal biomass. This effect strength is roughly conserved when GPP is indexed to biomass, suggesting that the effect occurs even where filamentous algae are not the dominant autotrophs. Finally, the effect is conserved when we consider the impacts of Fe enrichment on epiphytic algal biomass accrual on tiles. In each case, the effect is to stimulate growth, and in each case, the effect was strongest when considered along with covariates (e.g., cover for the effect of GPP, depth for the effect of epiphytic algal biomass). This supports a complex and nuanced view of the impacts of nutrient enrichment, but also focuses keen attention on Fe sources and cycling as an important knowledge gap in the aquatic ecology of Rainbow River.

Establishing Fe as a limiting nutrient in a Florida spring may not yet be warranted; further work is clearly needed to establish the generality and replicability of these findings. However, these results do support the prioritization of determining the spatial and temporal extent of Fe bioavailability and internal cycling. Moreover, considerations of Fe effects may be conjoined to other explanations for large-scale changes observed in Florida's springs. One explanation for changing autotroph cover includes low DO (Heffernan et al., 2010), principally via impacts to algal grazers, the loss of which under low DO conditions enables the accumulation of algal biomass. We note that Fe solubility increases under low redox conditions, such that lower DO likely increases Fe availability via reduction and solubilization from sediments (Reddy & DeLaune, 2008). The aquifer also contains large amounts of Fe that could theoretically be solubilized with a decrease in DO as many springsheds are under a confining layer (Hawthorn Formation) known for deposits of Fe (Springfield, 1966). This interaction could focus the origins of any Fe changes to aquifer consumption, which may preferentially use aquifer water at higher DO, thereby reducing average DO in the blended spring discharge (Heffernan et al., 2010). It is worth noting that DO in Rainbow Springs remains relatively high. While this points towards an aquifer management target (i.e., ensuring high DO to limit Fe mobilization), it is clearly not easily implemented. In Rainbow, the dynamics of Fe may be dominated by longitudinal changes in sediment availability, with particular attention needed for the increase in mine-tailings in the middle and lower river. If Fe availability has been modified by the presence of these sediments, and this has led to filamentous algal proliferation in the lower, but not upper, river, then some management options such as sediment stabilization or dredging may prove to be more plausible than previously thought.

Part 4.2 NO_3^- Uptake Dynamics

Methods

During several of the deployments we also deployed an in-situ spectrophotometer (SUNA; Satlantic, Halifax NS) inside the control chamber and set to record NO_3^- concentrations at 15 minute intervals (sample profiles Figure 5-1). This ensures that the fine-scale structure of the NO_3^- signal we observe is solely the result of localized processing and is unaffected by variation in delivery or by hydraulic transport. This allows us to more accurately examine the timing and magnitude of the overlapping constituent processing pathways. This also allowed us to determine how various NO_3^- uptake rates changed in response to NO_3^- depletion over time, i.e. the uptake kinetics. Understanding NO_3^- uptake kinetics, is critical because reaction kinetics determine how nutrient uptake will respond to changing concentrations (i.e. nutrient loading). Our understanding of reaction kinetics is primarily inferred from cross-site analysis (e.g. LINXII; Hall et al. 2009, Mulholland et al. 2009), however these analyses may be confounded by spatial heterogeneity in factors outside concentration which also influence uptake. Within-reach dynamics are difficult to ascertain, primarily because under natural conditions temporal concentration variation is typically limited. This constraint can be alleviated through artificial enrichment [e.x. Dodds et al., 2002, Payn et al., 2005], however this requires substantial time and effort and is impractical in certain settings, particularly larger streams and rivers [Ensign and Doyle 2006, Tank et al., 2008]. The concentration gradients we are able to produce here (~2 orders of magnitude) are larger than can be produced through artificial dosing of streams of even moderate size, and more critically we are able to examine kinetics at concentrations below ambient.

The rate of change in NO_3^- concentration (i.e. the profile slope) was multiplied by the chamber water depth (*d*) to calculate the observed net NO_3^- uptake rate (U_{NET}) in units of mg-N m^{-2} d^{-1}.

$$U_{NET} = \frac{\partial[NO_3^-]}{\partial t} \times d \times \frac{1000L}{m^3} \quad (4\text{-}1)$$

Using this connotation, negative values of U_{NET} indicate NO_3^- removal, while positive values indicate NO_3^- production. To account for sensor noise we used a three-point running average of concentration to calculate the derivative.

We then developed a numerical model for NO_3^- uptake based on assimilatory and dissimilatory pathways (Heffernan and Cohen 2010).

$$U_{model} = U_A + U_D \tag{4-2}$$

The model could have assumed temporal and stoichiometric coupling of UA with GPP: this declines in U_A as a result of NO_3^- concentration depletion would occur indirectly, vis-à-vis declining primary production (i.e. nutrient limitation). However it is possible that U_A may decline with concentration depletion while GPP does not. This may occur because autotroph uptake stoichiometry may be plastic, temporal decoupling between GPP and UA may occur (Appling and Heffernan 2014) and/or autotrophs may switch to an alternative source of N, for example NH_4+ (Peterson et al. 2001, Kemp and Dodds 2002). Thus the model relaxes the assumption of stoichiometric and temporal coupling of U_A with GPP. U_A is modeled as a power function of NO_3^- concentration and a generic daily half sine wave *hsin(t,τ)*. This half sign wave has an amplitude of one, a frequency of 24 hrs and a phase offset τ (t and τ in hrs). A positive value of τ indicates a peak lagging noon, while a negative value indicates a peak preceding noon.

$$U_{model} = -k_A[NO_3^-]^{n_A} hsin(t,\tau) - k_D[NO_3^-]^{n_D} \tag{4-3}$$

$$hsin(t,\tau) = \begin{cases} 0 & if\ t-\tau < 6 \\ \sin\left(\left(\frac{2\pi}{24}\right)t - \tau - 6\right) & if\ 6 \le t-\tau \le 18 \\ 0 & if\ t-\tau > 18 \end{cases} \tag{4-4}$$

Note that all the models contain only negative removal terms. Potential NO_3^- production pathways exist, namely nitrification. Our intent was to also include a positive nitrification term, however because of the dynamic between removal through U_D and production through nitrification, this class of model frequently converged on equi-final and/or implausible solution (removal and production rates which were roughly balanced, but each exceeded maximum values reported in the literature by orders of magnitude). This limitation of the model, its effect on inferred process rates, and potential methods of overcoming it will be an important Discussion point.

By minimizing the sum of squared errors (SSE) between the models and the observed U_{NET} in the benthic chambers using a Generalized Reduced Gradient algorithm implemented using the Solver function in Microsoft Excel, we solved for the optimal values of the unknown parameters for each model. Using the ratio of SSE to Total Sum of Squares (TSS), we also

calculated the coefficient of determination (R^2) as a metric of the observed variance captured by each model.

After determining the most parsimonious model which satisfactorily described the observed behavior, we created histograms of the distributions of model parameters, specifically the model exponents, n_A and n_D. This allowed us to examine the reaction kinetics of assimilatory and dissimilatory uptake pathways. We also plotted daily GPP, U_A and U_D versus NO_3^- concentration for each deployment to better visualize how these reaction rates change in response to concentration depletion. Finally, by converting GPP and U_A to molar units and assuming Net Primary Production = ½GPP (Hall and Tank 2003, Hall and Beaulieu 2013) we estimated an ecosystem autotrophic uptake C:N ratio. We compared this with the tissue stoichiometry of the dominant autotrophs present in these streams, which on a mol-C:mol-N basis ranged from roughly 8:1 to 18:1 (Zimba et al., 1993, Nifong et al., 2014), and inferred how uptake C:N ratios changed in response to NO_3^- depletion over the course of the deployments.

Results

NO_3^- profiles from Silver River, Rainbow River and Gum Slough exhibited declining concentrations with time (Figure 4-14), suggesting net removal of NO_3^- at incipient concentrations. While all of the profiles declined hyperbolically, the degree of inflection varied markedly; some profiles saw NO_3^- depleted by half in only a day or two, while others required an entire week. In addition to the global downward curvilinear trend, all profiles exhibited varying degrees of diel variation in profile slope, with daytime slopes generally steeper than nighttime slopes. The hyperbolic nature of the concentration profiles was clearly reflected in U_{NET} calculated from profile slopes (Figure 4-14), which declined with time. Diel variation in U_{NET} was also readily apparent, with generally higher rates in the day relative to the night.

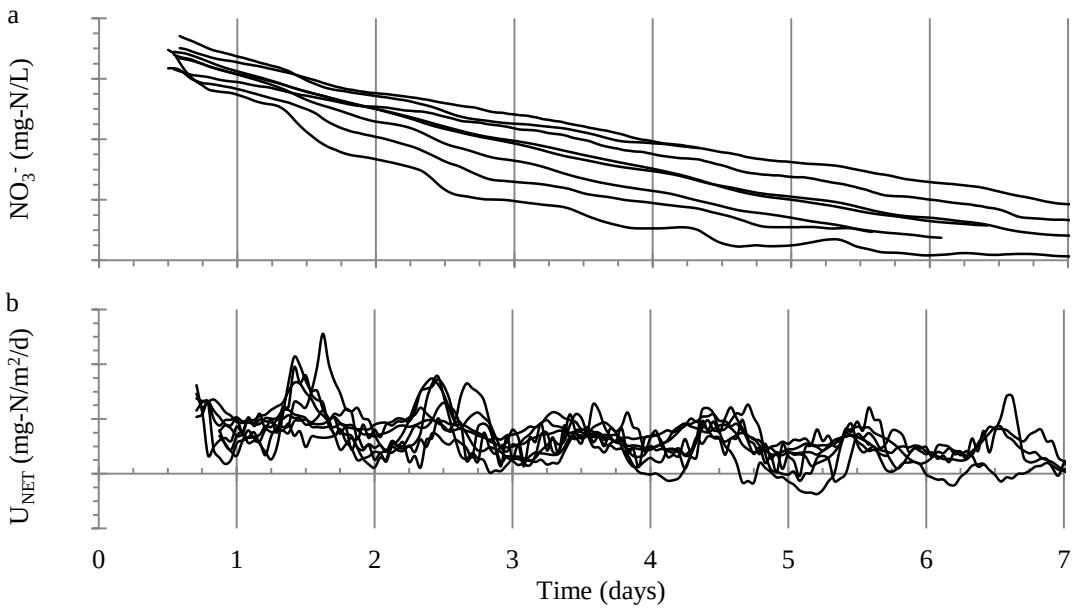

Figure 4-14. Control chamber NO_3^- profiles (top) and U_{NET} inferred from profile slope. Note U_{NET} is generally higher during the day as a result of UA.

The mean of fitted n_A values was 0.32, while the mean of n_D was 0.63, suggesting U_D to be the more concentration dependent pathway. Fitted n_A values are roughly evenly distributed between 0-1, while n_D values are skewed to larger values. The mean n_D value of 0.63 is only slightly higher than the exponent value (0.50) reported for denitrification across 72 streams in the LINXII experiment (Mulholland et al., 2009). The mean of fitted τ values lagged solar noon by 0.3 hrs suggesting U_A may perhaps slightly lag GPP, though this appeared to vary widely by deployment.

Table 4-10. Summary of fitted model parameter values.

Deployment start	n_A	n_D	τ	R^2
10/19/2015	0.67	0.50	10:14	0.78
10/26/2015	0.00	0.64	10:33	0.80
11/10/2015	0.00	0.35	10:35	0.58
5/24/2016	0.43	0.91	14:44	0.69
6/14/2016	0.43	1.00	11:52	0.79
2/14/2017	0.00	0.43	14:43	0.35
2/21/17	0.00	0.23	13:11	0.45
2/28/17	1.00	1.00	12:25	0.75

As with the previous chamber results, we observed no deleterious effect of NO_3^- depletion on rates of measured GPP (Figure 4-15a) over the course of deployments, suggesting NO_3^- is not a limiting nutrient even at low concentrations. While U_A generally declined with concentration (Figures 4-15c), it was much less pronounced than U_D (Figures 4-15d) consistent with U_D being the more concentration dependent pathway. As GPP remained relatively constant and U_A declined, the inferred autotrophic uptake C:N ratios increased as NO_3^- became depleted over the course of the deployments (Figure 4-15b).

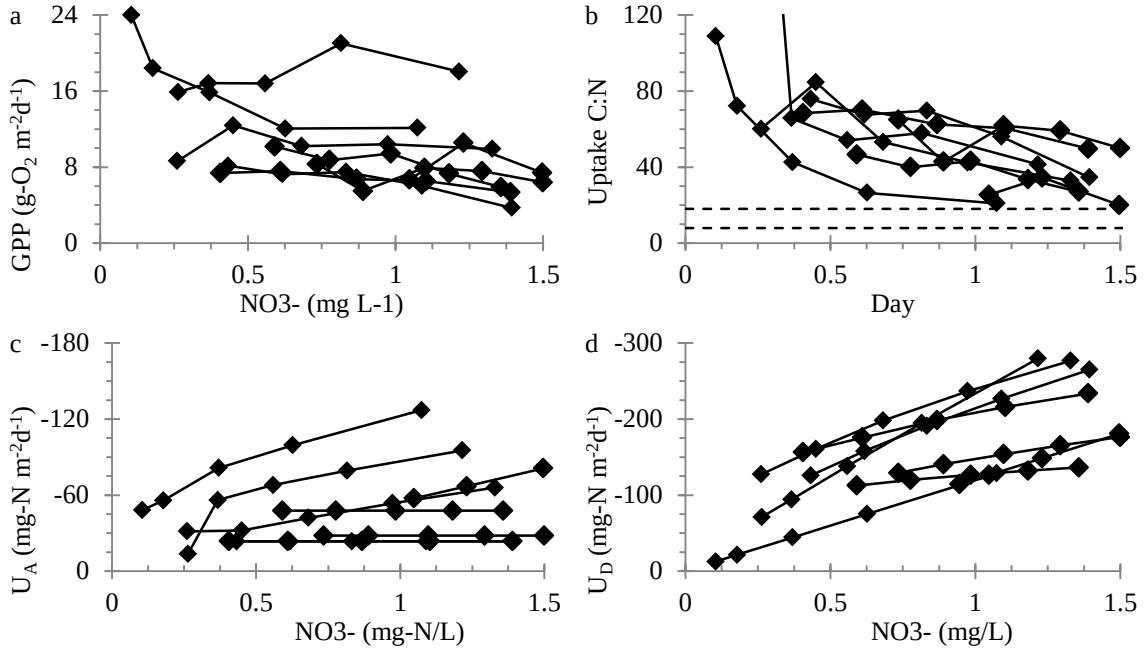

Figure 4-9. GPP (a), inferred uptake C:N (b), U_A (c) and U_D (d) versus NO_3^- concentration for each deployment. Dashed lines indicate range of observed tissue C:N.

The use of benthic chambers to isolate localized processing from hydraulic artifacts has the potential to reveal subtleties of processing signals which might otherwise be obscured by upstream delivery or hydraulic dispersion. For example, uptake rates inferred from open channel NO_3^- signals collected in similar settings using the same sensors (e.g. Heffernan and Cohen 2010) exhibit roughly sinusoidal diel variation. However the chamber profiles reveal that generally the diel variation in uptake rates is better modeled using a half-sine function evocative of solar insolation which is presumably driving assimilatory uptake vis-à-vis primary production. The more sinusoidal signals observed in the open channel are likely the result of hydraulic dispersion of this half-sine wave (Hensley and Cohen 2016).

The chambers also revealed slight offsets in the timing of maximum daily U_{NET} relative to maximum daily GPP circa solar noon. A slight lag had also been noted before (Heffernan and Cohen 2010, Kurz et al. 2014), but later interpreted to be potentially hydraulic (Hensley and Cohen 2016). Yet we still observe it in the chambers, where hydraulic transport effects have been removed. This may be a physiological offset between autotroph carbon fixation and nitrogen uptake, as has been observed for phosphorus (Cohen et al. 2013). However another possibility is that diel variation in U_{NET} does not exclusively represent U_A. Variation in the amplitude and timing of other pathways relative to the timing and amplitude of U_A has the potential to shift the timing of the combined U_{NET} signal forward or backward in time. Afternoon accumulation of DO from primary production may stimulate nitrification (an aerobic process) while also potentially inhibiting denitrification (an anaerobic process). This decline in net dissimilatory removal (or potentially even net production) would offset U_A producing a U_{NET} signal which peaked earlier than solar noon. Alternatively, accumulation of DOC or increased temperatures may stimulate afternoon denitrification (or heterotrophic uptake), producing a U_{NET} signal which peaks later than solar noon.

Finally, nighttime U_{NET}, while sloping downwards night to night over the course of the deployment in response to NO_3^- depletion, often slopes upward over the course of individual nights. This raises several intriguing possibilities. One is that NO_3^- removal through U_D is becoming stimulated as the DO accumulated over the course of the day through primary production is consumed during the night through respiration (denitrification is an anaerobic process). Alternatively, production of NO_3^- through nitrification (an aerobic process) is inhibited via nighttime DO depletion. In either case it further supports the conclusion that pathways other than U_A are also time varying.

The observation that GPP remained constant over the course of the deployments while NO_3^- declined suggests that NO_3^- is not a limiting nutrient of autotrophic growth in these systems. Constant GPP and decreasing U_A may suggest autotrophic uptake C:N ratios must be increasing (Figure 5b). As NO_3^- becomes depleted, autotrophs may modify their C:N uptake stoichiometry by internal recycling of N and building lower N tissue. However, analysis suggests tissue stoichiometry to be largely homeostatic (Nifong et al. 2014). It's more plausible the actual stoichiometry of autotrophic uptake does not change, just our inference based on our

assumptions. First, as water column NO_3^- becomes depleted, rooted macrophytes may obtain NO_3^- from hyporheic pore waters via their roots, which would not show up in the water column U_{NET} signal. We consider this possibility extremely unlikely as anoxic porewaters have likely been denitrified of NO_3^- (Kurz et al, 2015), and this source would not be available for non-rooted autotrophs such as benthic and water column algae. Second, we are only measuring NO_3^-. As this source becomes depleted, autotrophs may switch to an alternative source of N, namely NH_4^+. In fact alternative N sources may potentially be in use at ambient concentrations, as evident by the higher than expected C:N ratios observed even at the beginning of the deployments (Figure 4-9b). While measured NH_4^+ in the water column is typically at detection limits in these systems (Heffernan and Cohen 2010), this does not preclude, and may even suggest, it being rapidly assimilated. Finally, our estimates of U_A are based on diel variation. At low N concentrations autotrophic assimilation may become decoupled from primary production such that N uptake is occurring continuously and not on a diel basis. Additionally, temporal variation in other processing pathways may influence the net amplitude of the diel signal. Thus simply using the diel signal may not be sufficient to infer total assimilatory N uptake. In conclusion, just as enrichment with NO_3^- produces no noticeable effect on rates of GPP, so too does NO_3^- depletion.

Part 4.3 Chamber NH_4^+ Addition

Methods

To further understand the role of N-species other than NO_3^-, we performed several additional paired chamber deployments. One chamber served as a control, while the second chamber was initially dosed with NH4+ up to a concentration of 2 mg-N/L as NH_4^+. A SUNA to measure NO_3^- and HOBO to measure DO were positioned in both boxes to calculate the response of NO_3^- uptake and GPP to NH4+ addition. We performed eight successful deployments (deployments where both the treatment and control boxes did not leak), each lasting one week.

Results

The results suggest that addition of NH_4^+ significantly alters NO3- processing dynamics. In particular, addition of NH_4^+ reduces net NO_3^- uptake such that concentrations remain elevated,

in many cases for the duration of the weeklong deployments. Control versus treatment NO_3^- profiles for the deployments are shown below in Figure 4-16.

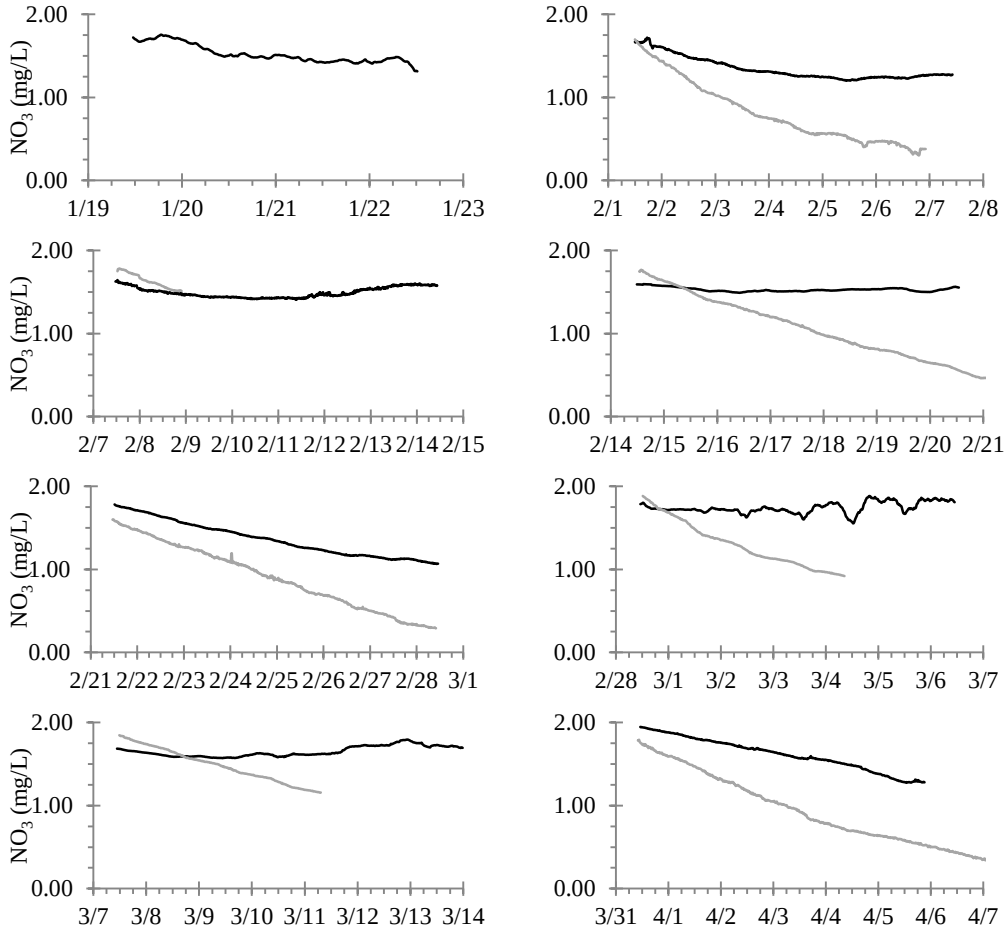

Figure 4-10. NO_3^- profiles from control (gray) versus NH_4^+ addition (black) chambers. Addition of NH_4^+ significantly reduces net uptake of NO_3^-.

Reduced net uptake can occur through a combination of mechanisms. Assimilatory uptake of NO_3^- may be reduced as NH_4^+ is preferentially assimilated. Alternatively, NH_4^+ addition may stimulate NO_3^- production through nitrification. There is nothing in the literature to suggest NH_4^+ inhibits NO_3^- removal through denitrification.

A comparison of U_{NET} for deployments where we have both control and treatment profiles is shown in Figure 4-17 (Note for two deployments the control chamber SUNAs failed, however we believe it is fairly safe to assume that the NO_3^- uptake dynamics in these control chambers would be consistent with that observed in control chambers during later deployments, as well as that observed in the control chambers for the nutrient assays, i.e. previous section).

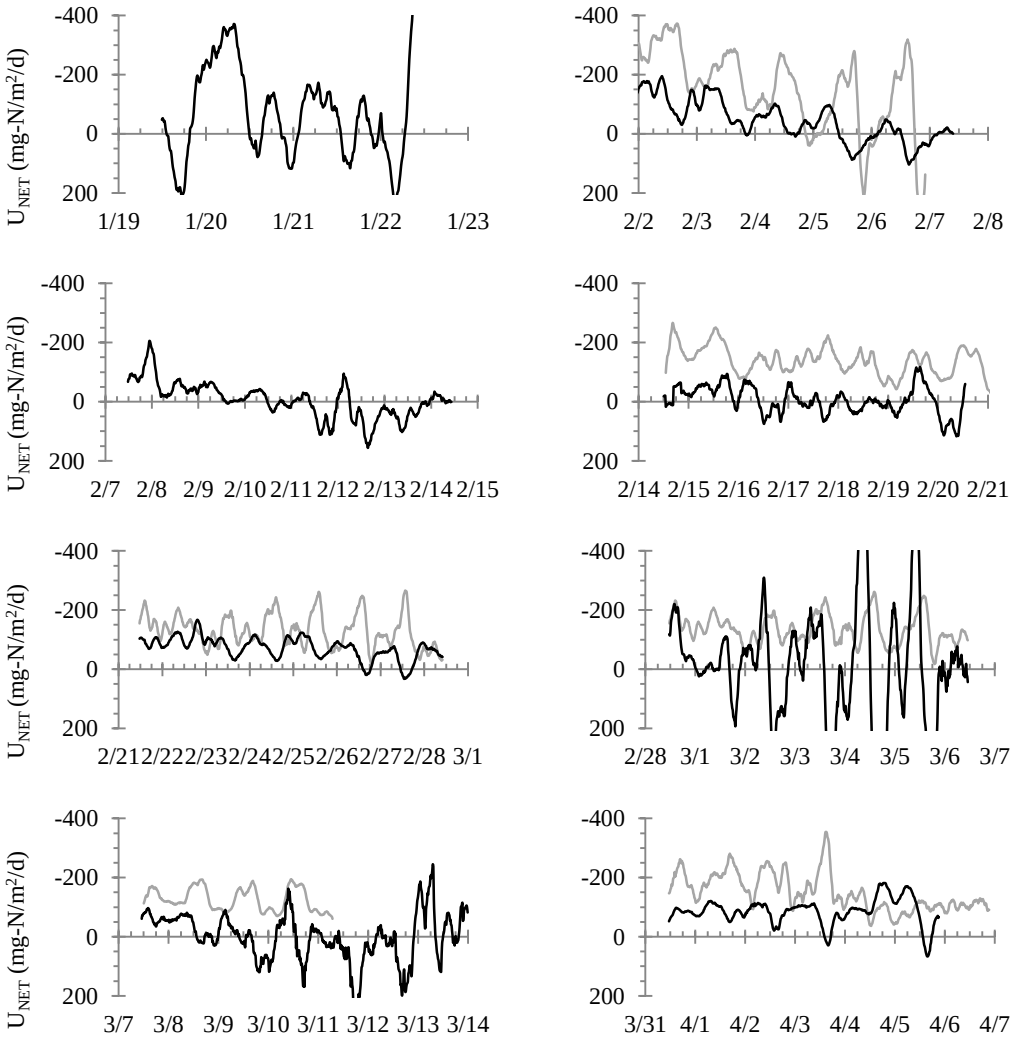

Figure 4-11 U_{NET} for control (gray) and NH_4^+ addition (black) chambers.

Control chamber dynamics were similar to what we observed in the previous section, with net uptake generally decreasing over the course of the deployments, and daytime peaks in uptake roughly synchronous with primary production, suggesting coupled assimilatory uptake. Treatment chamber responses were more varied across deployments. In general, treatment chambers exhibited lower U_{NET} than their corresponding control chamber. At many times treatment chamber U_{NET} exhibited positive values indicative of net enrichments (i.e. increasing NO_3^- concentrations). While treatment chamber U_{NET} did often exhibit diel variation, in most instances the phase was offset from that observed in the corresponding treatment chamber. Most of the treatment chambers exhibited peak daily U_{NET} values at night, with net removal during the day being lower. Because we have little reason to believe that autotrophic uptake would

preferentially occur at night, when primary production is not occurring, we do not believe this diel variation to be assimilatory. Instead, we speculate that daytime production of DO through photosynthesis may be stimulating nitrification of the added NH_4^+ into NO_3^- (this process may be occurring continuously, but as an aerobic process may be enhanced during the day).

This increased production of NO_3^- through nitrification partially (or almost entirely in a few deployments) balances removal through denitrification such that less (or no in a few deployments) net removal occurs in the treatment chambers relative to the control chambers. We were quite surprised that this could be maintained for so long (at least a week in some cases) given only a modest amount of NH_4^+ was added, and only at the beginning of each deployment. Post-deployment grab samples were collected from each chamber to be analyzed for NH_4^+ to determine how much net conversion to NO_3^- occurred, however these results are not available at the time of this report.

As with the other nutrient additions, we did not observe any significant effect of NH_4^+ addition on GPP. Control and treatment chamber mean GPP for each deployment is shown in Figure 4-18. Pooled across all deployment mean GPP for the control and treatment chambers were virtually identical, 5.31 g-O_2/m^2/d. We also did not observe any changes in treatment chamber GPP over the course of the deployments as added NH_4^+ was presumably depleted. Together, this strongly suggests that in this system NH_4^+ addition does not stimulate GPP.

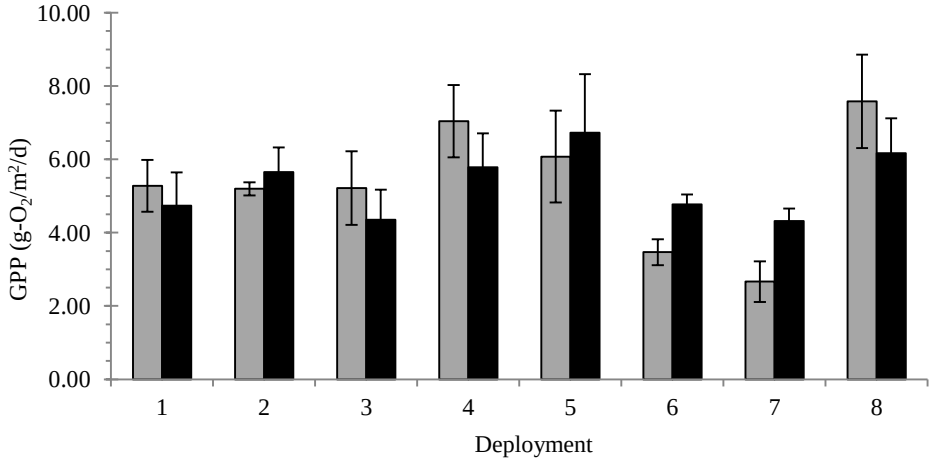

Figure 4-12 Mean GPP in control (gray) versus NH_4^+ treatment (black) chambers for each deployment.

Section 5. Vegetation transplant

Methods

We noted previously (Part 1) there is a marked transition in the distribution of aquatic vegetation in Rainbow River which generally corresponds with a transition in sediment type. Here we sought to answer whether the gradient in sediment type was potentially driving differences in vegetation, or whether vegetation distribution was controlled by some other longitudinally varying factor such as water chemistry or light transmittance. To do this we performed a vegetation transplant study.

We chose three species of vegetation commonly found in Rainbow River (*Sagittaria kurziana*, *Vallisneria americana* and *Hydrilla verticillata*), four substrate types (sandy, flocculent organic, and clay from Rainbow River, plus a low-P bentonite clay), and two locations (upstream and downstream). Sand was collected near the outlet of Indian Creek (29.090°N, 82.426°W). Organic sediments were collected from the channel margin just downstream of this location. Clay sediments were collected from just upstream of the inlet to Blue Cove (29.055°N, 82.446°W). We also used a low-P clay in addition to the naturally occurring clay from Rainbow River to test whether it was the clay texture or the chemical composition which was potentially influencing SAV distribution. The upstream location was located at 29.090°N, 82.426°W while the downstream location was located at 29.045°N, 82.455°W. Overall, 72 pots were deployed, with three replicates of each sediment texture, species, and location. The plants were transplanted, bare-root, into 30 cm diameter terracotta pots filled with one of four sediment types. After a month adjustment period to minimize transplant shock, transplants were trimmed to 20 cm above ground to establish a baseline for future growth measurements. After three months, the plants were trimmed back to 20 cm. Plants were then grown for another three months, at which time a destructive harvest was completed. Plants were transplanted November 30th 2015 with a harvest in March and July 2016.

Harvested plant material was returned to the lab where the number of shoots, shoot length, and dry biomass weight were used as plant vigor metrics for *S. kurziana* and *V. americana*. Length was measured as the longest portion of a shoot. Dry mass was weighed after 24 hours in a drying oven at 80°C. Results were reported on mass or length increase per shoot

per day to control for different starting plant sizes and slight differences in time between clippings. For *H. verticillata* length estimates were unreliable and only mass was recorded. The number of stems harvested could also not be measured. Fortunately, all *H. verticillata* plants began at the same size and had uniform stems, making reporting on a per shoot basis unnecessary and mass/day an adequate metric. A direct comparison between *S. Kurziana/ V. Americana* and *H. verticillata* growth was not possible due to the lack of shoots.

Figure 5-1. Clipped Vallisneria americana.

Analysis of variance (ANOVA) was completed using R for each species specific dataset. We considered the main effects of sediment type, species, location and harvest data, as well as their interactions, on both growth responses (i.e., mm or mg per day per shoot). A post-hoc Tukey HSD was performed to assess differences among treatments. Because of the low sample size and the relatively low risks of Type II error, we adopted a 90% significance criterion ($p < 0.10$) for determining significant treatment effects.

Results

The final dataset included both mass (mg) and length (mm) datasets for above ground biomass accumulation on a per day, per shoot basis of both *S. Kurziana* and *V. Americana*, and mg/day for *H. verticillata*. Growth data were obtained only for plants present at the time of clipping. A substantial number of plants disappeared between visits; potentially the result of either transplant shock, wildlife activity, scouring or vandalism. Vandalism at the downstream site before the second clipping (July) destroyed 28 plants (nine *S. kurziana*, seven *V. americana*, and 12 *H.*

verticillata). Apart from this, "natural" loss of six transplants occurred for *S. kurziana*, five for *V. americana*, and 21 for *H. verticillata*. This reduced the desired overall sample size by 19%, from 144 plants to 116. Nevertheless, strong explanatory effects were still obtained from the data, although the power to compare and assess seasonal effects was reduced. For *S. kurziana* and *V. americana*, samples lost occurred primarily in bentonite clay, while *H. verticillata* samples were lost relatively evenly across substrates (Figure 5-2).

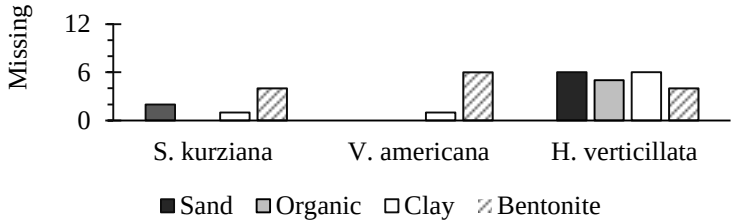

Figure 5-2. Number of missing plants by sediment type (Chi-sq p-value=0.129, 0.004, 0.739, from left to right). Does not include deliberate vandalism.

The growth rate between study species was compared in order to determine overall plant changes in length or biomass. For growth per day (not weighted to number of shoots); *S. kurziana* averaged 7.75 mm day^{-1} and 1.64 mg day^{-1} of growth; *V. americana* averaged 26.28 mm day^{-1} and 13.05 mg day^{-1} of growth; and *H. verticillata* averaged 9.07 mg day^{-1} of growth (Figure 5-3A,B). However, *S. kurziana* had systematically lower stem density than V. americana. When these shoot density differences were considered *S. Kurziana* averaged 1.42 mm day-1 shoot-1 and 0.29 mg day^{-1} shoot^{-1} of growth; *V. americana* averaged 1.37 mm day-1 shoot-1 and 0.62 mg day^{-1} of growth (Figure 5-3C,D).

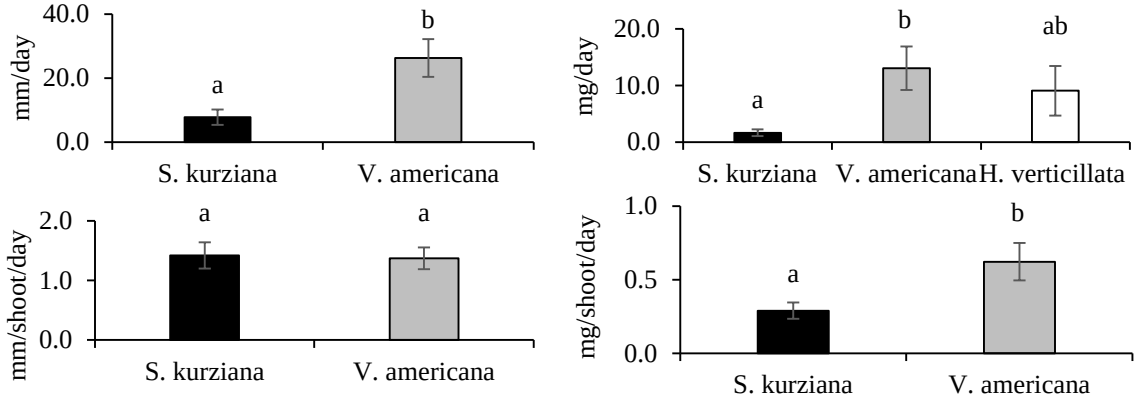

Figure 5-3. Growth differences between species across all conditions. A) Difference in shoot elongation between S. kurziana and V. americana is significant (p<0.001) B) Significance varies

between species for growth measured by mass - S. kurziana-V. americana (p<0.001), S. kurziana-H. verticillata (p=0.009), V. americana-H. verticillata (p=0.371) C) Difference in elongation between S. kurziana and V. americana is not significant (p=0.936) D) Difference in growth measured by mass between S. kurziana and V. americana is significant (p<0.001). Error bars represent 95% confidence intervals. Differing letters above bars indicated a p-value <0.05 between the two.

The main effect of sediment was significant (p<0.001) for growth of *S. kurziana* for both length (Figure 5-4A) and mass (Figure 5-4B). The response of *V. americana* to sediment type was not significant for length (p=0.141), and was only marginally significant for mass (p=0.074). *H. verticillata* growth (note: only a mass basis, mg d^{-1}) was not significantly impacted by sediment type (p=0.371) (Figure 5-4).

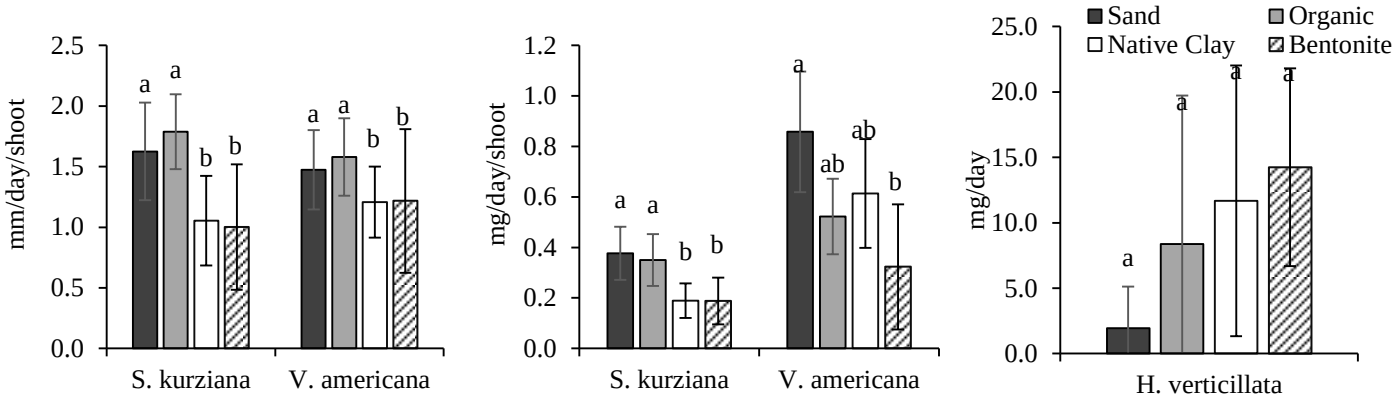

Figure 5-4. Growth measures of the three plant species in each of the four sediment types. P-values for A) S. kurziana elongation (<0.001), V. Americana elongation (0.141), B) S. kurziana mass (0.001), V. Americana mass (0.074), and C) H. verticillata mass (0.371). Error bars represent 95% confidence intervals. Differing letters above bars indicated a p-value <0.05 between the two.

Tukey's HSD post-hoc analysis indicated two groups of sediment types for *S. kurziana*, with sand and organic sediments inducing the same high growth, and a clay group (native clay and bentonite) supporting low growth. The only significant pairwise contrast for *V. americana* was between sand and bentonite measured by mass. *H. verticillata* exhibited no significant responses to sediment.

To assess the different light levels and water column P concentrations, two different locations were utilized. *S. kurziana* and *V. americana* showed no significant effects of location on length measurements (p=0.396, 0.141, respectively). However, a difference in growth as determined by a change in mass was significant for *V. americana*, which showed an increase in

growth at the downstream location (0.074). The effects of location on mass growth of *S. kurziana* (p= 0.51) and *H. verticillata* (mg day-1, p = 0.70) were not significant (Figure 5-5) (Table 5-1).

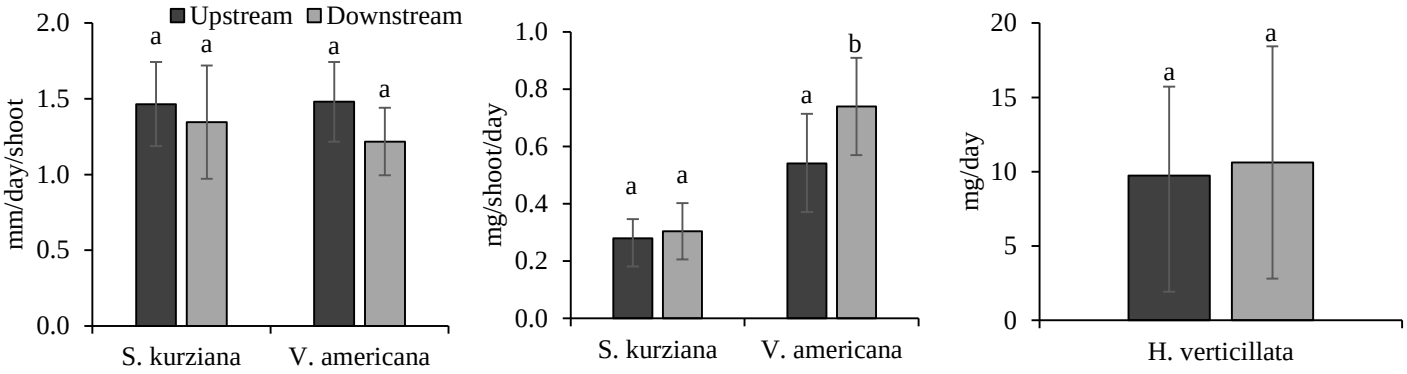

Figure 5-5. Growth measures of the three plant species in each of the two locations. P-values for A) S. kurziana elongation (0.396), V. Americana elongation (0.141), B) S. kurziana mass (0.510), V. Americana mass (0.074), and C) H. verticillata mass (0.700) from left to right. Error bars represent 95% confidence intervals. Differing letters above bars indicated a p-value <0.05 between the two.

Two separate time periods were assessed with harvest in March and July; March-July data were only available for the upstream location. *S. kurziana* exhibited a significant change in growth between time periods as indicated by both length and mass growth (p<0.000). *V. americana* did not exhibit a significant change in mass between the two time periods (p=0.297), but a growth difference was evident on a mass basis (p=0.036) (Figure 5-6). No *H. verticillata* were harvested in July (upstream were all missing due to natural loss while downstream had been vandalized).

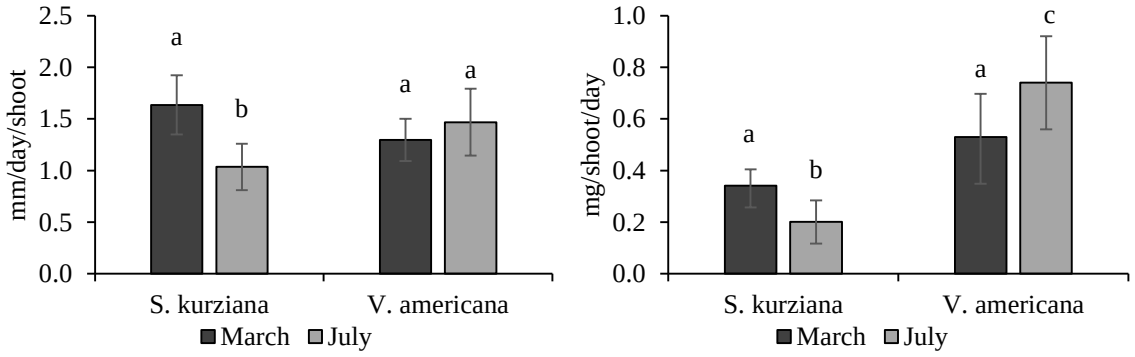

Figure 5-6. Growth measures by harvest month. A) The second S. kurziana harvest was significantly smaller for length (P<0.001). V. americana did not vary significantly between

harvests for length (P=0.297). B) The second S. kurziana harvest was significantly smaller for mass (P<0.001). V. americana varied significantly between harvests for mass (p=0.036). No H. verticillata specimens were alive for the July harvest. Error bars represent 95% confidence intervals. Differing letters above bars indicated a p-value <0.05 between the two.

Plant loss in bentonite clay replicates was much greater than in other sediment types. Bentonite clay became increasingly flocculent with time and appeared to be susceptible to erosion, likely explaining differences in survivorship between it and the native clay. *Hydrilla verticillata* experienced a causality rate much higher than the other two species across all sediment types, potentially due to transplant stress; this is surprising given its invasive nature and ability to spread quickly from propagule fragments. The evidence firmly points towards bentonite clay being poor for rooted macrophyte growth, even more so than the naturally occurring clay found in Rainbow River.

Growth differences among the study species were strong. Across all treatments, *V. americana* grew (i.e., increased mass) most rapidly, followed by *H. verticillata*, and finally *S. kurziana*. A similar ranking was shown for elongation. This suggests that overall, *V. americana* is likely the most productive species in these conditions. When weighted for shoot density, *S. kurziana* and *V. americana* elongated at similar rates, an artifact of *V. americana* tending to spread laterally and produce new clones (Xiao et al., 2007). While elongation per shoot was similar between the two species, thicker and wider shoots typical of *V. americana* resulted in dramatic differences in mass accrual per shoot in comparison to *S. kurziana*. Attempting to scale individual plant growth to a per area basis, as used in other Florida spring SAV growth studies, is not reliable given variable stocking densities, making growth comparison to other published rates (Dutoit, 1979; Odum, 1957b,) difficult. Hauxwell (et al. 2001) estimated per shoot growth rates of *V. Americana* peaking at 50 mg/shoot/day, which was extremely higher than what we measured in our transplanted plants.

The two study sites, upstream and downstream, were selected to assess the potential effects of light availability on plant growth. Blue light availability has been shown previously to exert a strong control on SAV growth in the Rainbow River (Szafraniec, 2014). No detriment in growth was noted at the downstream location for any treatment, or combination thereof. The study design necessitated the installation of transplants in less than half a meter of water (to avoid the use of SCUBA) and likely obscured true differences in the light regime between the

two sites. *Vallisneria americana* did experience a significant increase in growth downstream when expressed as mg day^{-1} $shoot^{-1}$, a trend opposite of what was expected. Additionally, there were likely differences in light reaching the water surface. The upstream station was located closer to the channel bank, and therefore potentially received greater shading from riparian vegetation. Light was not the only difference between the two sites, another co-variable could be responsible, such as elevated surface P concentration at the downstream site. The mechanism in which this would occur, as the previous section suggested deleterious effects of P to *S. kurziana*, is unclear.

The two harvests involved growing periods during seasons with different lengths of daylight, but the summer season did not result in a general increase in plant growth. In fact, *S. kurziana* exhibited a significant decrease in growth before the July harvest. This may be the result of an inadequate sample size, as the July harvest resulted in about half of the amount of data as the March harvest. Alternately, the two different seasons of best growth could be due to morphological differences between the two species, as the March harvest may have captured rapid spring growth of *S. kurziana* and *V. americana* may change growth rate during a different time of the year.

The poor growth *S. kurziana* displayed in clay lends evidence to the hypothesis that sediment texture is, in part, responsible for the longitudinal shift in benthic coverage, from *S. kurziana* to *V. americana* and *H. verticillata*, observed in the study site. Sediment effects were weak for *V. americana* growth and not significant at all for *H. verticillata*, as might be expected of a versatile invasive. No significant difference was noted between the native clay and bentonite for any species, indicating that porewater P does not affect growth. The reduced vigor of S. kurziana in clay may allow the opportunity for *V. americana* and *H. verticillata* to colonize the downstream reaches.

Addendum

We performed as second vegetation transplant experiment beginning in December 2016. The experiment design was slightly modified to overcome some of the shortcomings of the first experiment. First, we selected two upstream and two downstream locations in an attempt to limit site-specific effects confounding upstream versus downstream analysis. Second, the results of

the initial experiment showed no significant difference between the natural clay sediments from Rainbow River and the low-P bentonite clay. There was also not a substantial effect of organic sediments. Therefore the second experiment utilized only two sediment types, sand and clay, both from Rainbow River, but with more replicates. At each of the four sites we performed four replicates of each of the six species-sediment combinations, for a total of 96 individual plants.

Transplanting occurred December 13, 2016. Replicates were positioned in a 6x4 grid, in a repeating pattern; this way species-sediment combinations were evenly distributed throughout the site versus clustered together, eliminating the potential for spatial effects (e.g. greater scouring or herbivory on the outer rows). After one month to establish, on January 10, 2017 we returned to perform the initial clipping. At this time, we discovered one of the upstream sites, opposite and slightly downstream of KP Hole park, had been completely destroyed by vandalism. The majority of pots had been pulled out of the ground and smashed. As it would need another month to establish before initial clipping, and then continuously lag behind the other three sites, we chose not to replace this site and continue the experiment with only one upstream site.

On April 4, 2017 we returned to measure growth over the intervening 3 month period. We discovered that the remaining upstream site, and one of the two downstream sites had been heavily disturbed. No pots were smashed this time but the majority had been pulled out of the ground and toppled. Many, though not all, of the disturbed pots still contained their plants (Figure 5-8), and we clipped and collected what biomass remained in an attempt to salvage the experiment. A cursory analysis of the results is shown in Figure 5-9.

Figure 5-8. Disturbed potted plants at downstream site 1 in April 2017. Note many plants were stilling growing in dislodged pots, however it was impossible to determine the effect of this disturbance on growth rates.

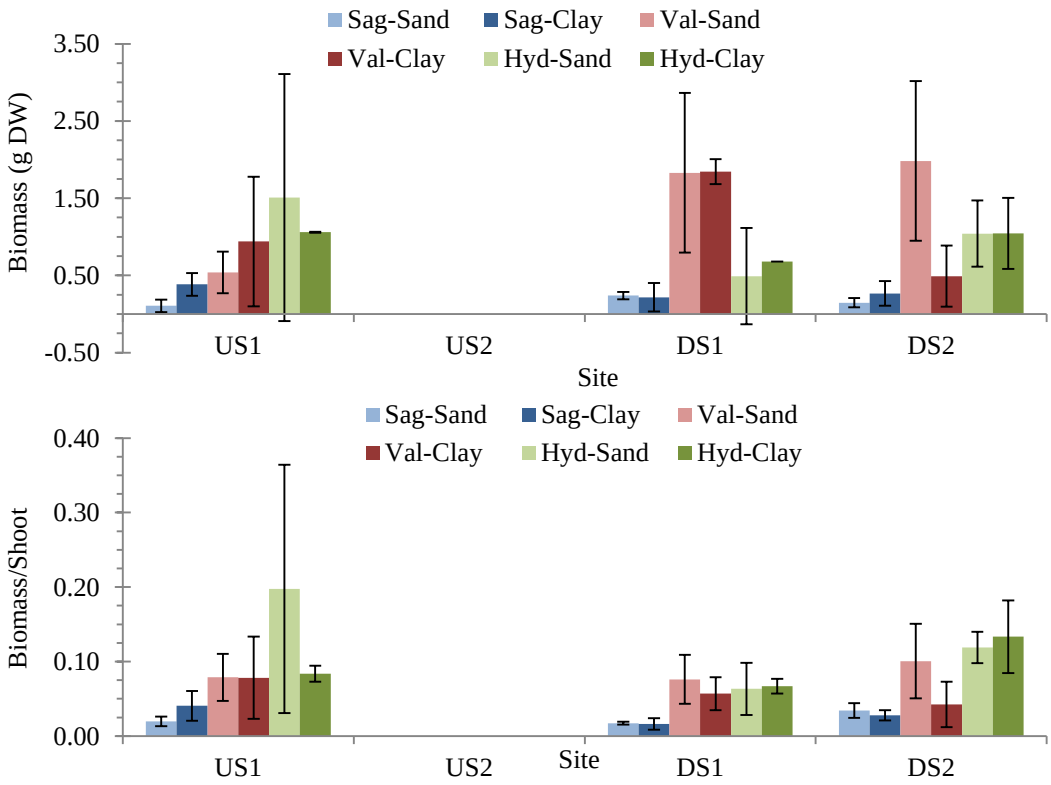

Figure 5-9 Growth from January to April 2017, in biomass (top) and normalized to number of shoots (bottom). Note upstream site 2 was destroyed before experiment commenced.

Note the large error bars in many instances because few replicates of a treatment survived; in some cases error bars cannot be calculated because only a single replicate survived. Also, it was impossible to determine which pots missing plants were due to disturbance, or natural mortality. Additionally, it was impossible to tell what sub-lethal effect the disturbance may have had on plant growth rates, and if this affect was equal across species. We caution drawing any conclusions from these results, and they are presented as an addendum rather than as part of the main section. Finally, the remaining undisturbed downstream site was allowed to continue to grow for a second three month period, however when we returned again in July, it too had been nearly completely destroyed by vandalism. This time we did not collect any samples as we felt the uncertainty in any potential results outweighed the effort in doing so.

One note we will make, is that at least visually, it appeared that *Vallisneria* survived best in pots which had been disturbed (i.e. no longer upright in their original position), while *Hydrilla* survived worse. There are also several takeaways as far as experimental design. During the first transplant experiment we placed signs near the transplant plots stating "Research in Progress, Please Do Not Disturb". Feeling that this may have drawn attention to the plots and let to vandalisms we went attempted a more discrete approach for the second attempt. It clearly did not have the desired outcome. In hindsight, disturbance to our plots seemed to occur right around peak recreational activity (i.e. Christmas Break, Spring Break, Summer Break) when more people our out on the river and likely to encounter them. We do note that we also performed over 50 deployments of the benthic chambers over a period of nearly two years and never experienced any vandalism. Although given the near universality it was hard to believe plot destruction was not intentional, it is possible that the damage may have been the result of boat propellers. During periods of heavy recreation (tubing and kayaking) motorized watercraft may be forced to navigate in shallower areas. This further highlights that recreational activity (motorized or otherwise) should not be discounted as an important influence on submerged vegetation.

Acknowledgements

Funding for this project came from the Southwest Florida Water Management District contract grant W420. We give special thanks to Sky Notestein and Sean King from SWFWMD. We thank Christine Housel and the Florida Department of Environmental Protection Division of Parks and Recreation for providing a research permit. We thank Larry Steed, Bob Dampan and Jeff Sowards, the staff of Rainbow Springs State Park, Rainbow Springs Aquatic Preserve and especially KP Hole County Park for facilitating site access.

References Cited

Atkins North America, Inc. (2012). 2011 Rainbow River Vegetation Evaluation. Prepared for Southwest Florida Water Management District. Brooksville, Florida.

Bott, T. L., J. T. Brock, C. E. Cushing, S. V. Gregory, D. King, and R. C. Petersen. 1978. A comparison of methods for measuring primary productivity and community respiration in streams. Hydrobiologia 60: 3-12.

Bott, T. L., J. T. Brock, C. S. Dunn, R. J. Naiman, R. W. Ovink, and R. C. Petersen. 1985. Benthic community metabolism in four temperate stream systems: an inter-biome comparison and evaluation of the river continuum concept. Hydrobiologia 123: 3-45.

Canfield, D. E., & Hoyer, M. V. (1988). Influence of Nutrient Enrichment and Light Availability on the Abundance of Aquatic Macrophytes in Florida Streams. Can. J. Fish. Aquat. Sci., 45(October 1984), 1467–1472. http://doi.org/10.1139/f88-171

Cohen, M. J., M. J. Kurz, J. B. Heffernan, J. B. Martin, R. L. Douglass, C. R. Foster, and R. G. Thomas. 2013a. Diel phosphorus variation and the stoichiometry of ecosystem metabolism in a large spring-fed river. Ecological Monographs 83: 155-176

Cohen, M.J., J.B. Heffernan, A. Albertin, R. Hensley, M. Fork, C. Foster and L. Korhnak. 2013b. Mechanisms of nitrogen removal in spring-fed rivers, Saint Johns River Water Management District Special Publication 2013-SP2.

Cowell, B. C., & Botts, P. S. (1994). Factors influencing the distribution, abundance andgrowth of Lyngbya wollei in central Florida. Aquatic Botany, 49, 1-17.

Cowell, B. C., & Dawes, C. J. (2008). Seasonal Comparisons of the Phytoplankton and Decline in Water Transparency in the Spring-Fed Rainbow River, Florida. Journal of Freshwater Ecology, 23(2), 169–177. http://doi.org/10.1080/02705060.2008.9664188

Dodds, W.K. et al. 2002. N uptake as a function of concentration in streams. Journal of the North American Benthological Society 21: 206–220

Doyle, W.M. and S.H. Ensign. 2009. Alternative reference frames in river system science. BioScience 59:499-510.

Duarte, C. M., & Canfield, D. E. (1990). Macrophyte standing crop and primary productivity in some Florida spring-runs. Journal of the American Water Resources Association, 26(6), 927–934.

Dutoit, C. H. (1979). Carrying capacity of the Itchetucknee Springs and River. University of Florida.

Ensign, S. H. and M. W. Doyle. 2006. Nutrient spiraling in streams and river networks. Journal of Geophysical Research. 111: G04009, doi:10.1029/2005JG000114

Hall, R. O., and J.L. Tank. 2003. Ecosystem metabolism controls nitrogen uptake in streams in Grand Teton National Park, Wyoming, Limnology and Oceanography, 48, 1120-1128, doi:10.4319/lo.2003.48.3.1120

Hall, R. O. et al. 2009. Nitrate removal in stream ecosystems measured by 15N addition experiments: Total uptake. Limnology and Oceanography 54: 653–665

Hall Jr, R. O., and J. J. Beaulieu. 2013. Estimating autotrophic respiration in streams using daily metabolism data, Freshwater Science, 32, 507-516, doi:10.1899/12-147.1

Hansmann, E., Lane, C., & Hall, J. (1971). A Direct Method of Measuring Benthic Primary Production in Streams. Limnology and Oceanography, 822–826.

Hauxwell, J., Cebrian, J., Furlong, C., & Valeila, I. (2001). Macroalgal Canopies Contribute to Eelgrass (Zostera marina) Decline in Temperate Estuarine Ecosystems. Ecology. http://doi.org/10.1890/0012-9658(2001)082

Heffernan, J. B., and M. J. Cohen. 2010. Direct and indirect coupling of primary production and diel nitrate dynamics in a subtropical spring-fed river Limnology Oceanography 55: 677–688

Heffernan, J. B., Cohen, M. J., Frazer, T. K., Thomas, R. G., Rayfield, T. J., Gulley, J., … Graham, W. D. (2010). Hydrologic and biotic influences on nitrate removal in a subtropical spring-fed river. Limnology and Oceanography, 55(1), 249–263. http://doi.org/10.4319/lo.2010.55.1.0249

Heffernan, J. B., Liebowitz, D. M., Frazer, T. K., Evans, J. M., & Cohen, M. J. (2010). Algal blooms and the nitrogen-enrichment hypothesis in Florida springs: evidence, alternatives, and adaptive management. Ecological Applications : A Publication of the Ecological Society of America, 20(3), 816–29.

Hensley, R. T., & Cohen, M. J. (2012). Controls on solute transport in large spring-fed karst rivers. Limnology and Oceanography, 57(4), 912–924. http://doi.org/10.4319/lo.2012.57.4.0912

Hensley, R. T., Cohen, M. J., & Korhnak, L. V. (2014). Inferring nitrogen removal in large rivers from high-resolution longitudinal profiling. Limnology and Oceanography, 59(4), 1152–1170. http://doi.org/10.4319/lo.2014.59.4.1152

Hensley, R. T., M. J. Cohen, and L. V. Korhnak. 2015. Hydraulic effects on nitrogen removal in a tidal springfed river. Water Resources Research 51: 1443–1456

House, W. a. (1990). The prediction of phosphate coprecipitation with calcite in freshwaters. Water Research, 24(8), 1017–1023. http://doi.org/10.1016/0043-1354(90)90124-O

Hoyer, M., Frazer, T., & Notestein, S. (2004). Vegetative characteristics of three low-lying Florida coastal rivers in relation to flow, light, salinity and nutrients. Hydrobiologia, 528(1999), 31–43. http://doi.org/10.1007/s10750-004-1658-8

Johnson, L. T., Tank, J. L., & Dodds, W. K. (2009). The influence of land use on stream biofilm nutrient limitation across eight North American ecoregions. Canadian Journal of Fisheries and Aquatic Sciences, 66(7), 1081–1094. http://doi.org/10.1139/F09-065

Kurz, M. J., de Montety, V., Martin, J. B., Cohen, M. J., & Foster, C. R. (2013). Controls on diel metal cycles in a biologically productive carbonate-dominated river. Chemical Geology, 358, 61–74. http://doi.org/10.1016/j.chemgeo.2013.08.042

Kurz, M.J., J.B. Martin, M.J. Cohen and R. Hensley. 2015. Diffusion and seepage-driven element fluxes from the hyporheic zone of a karst river. Freshwater Science 34:206-221

Lepp, P. W., and T. M. Schmidt. 1998. Nucleic acid content of *Synechococcus spp*. during growth in continuous light and light/dark cycles. Archives of Microbiology 170:201–207.

Mumma, M. T., Cichra, C. E., & Sowards, J. T. (1996). Effects of recreation on the submersed aquatic plant community of Rainbow River, Florida. Journal of Aquatic Plant Management, 34, 53–56.

Mullholand, P. J. et al. 2008. Stream denitrification across biomes and its response to anthropogenic NO_3^- loading. Nature 452: 202–205

Mulholland, P. J., et al. 2009. Nitrate removal in stream ecosystems measured by 15N addition experiments: denitrification. Limnology and Oceanography 54: 666-680.

Munch, D. A., et al. 2006. Fifty-year retrospective study of the ecology of Silver Springs, Florida, St. Johns River Water Manage. Dist. Publ. SJ2007-SP4, St. Johns River Water Manage. Dist., Palatka, Fla.

Nifong, R. L., Cohen, M. J., & Cropper, W. P. (2014). Homeostasis and nutrient limitation of benthic autotrophs in natural chemostats. Limnology and Oceanography, 59(6), 2101–2111. http://doi.org/10.4319/lo.2014.59.6.2101

Notestein, S. K., Frazer, T. K., Hoyer, M. V., & Canfield, D. E. (2003). Nutrient Limitation of Periphyton in a Spring-Fed, Coastal Stream in Florida, USA. Journal of Aquatic Plant Management, 41, 57–60.

O'Brien, J. M., W. K. Dodds, K. C. Wilson, J. N. Murdock, and J. Eichmiller. 2007. The saturation of N cycling in Central plains streams: 15N experiments across a broad gradient of nitrate concentrations. Biogeochemistry 84: 31–49

Odum, H. T. 1956. Primary production in flowing waters, Limnology and Oceanography 1: 102–117

Odum, H. (1957a). Trophic structure and productivity of Silver Springs, Florida. Ecological Monographs, 27(1), 55–112. Retrieved from http://www.jstor.org/stable/1948571

Odum, H. T. (1957b). Primary production measurements in eleven Florida springs and a marine turtle-grass community. Limnology and Oceanography, 2(2), 85–97. http://doi.org/10.4319/lo.1957.2.2.0085

Osborne, T., Mattson, R., & Coveney, M. (2015). Potential for Direct Nitrate-Nitrite Inhibition of Submerged Aquatic Vegetation (SAV) in Florida Springs: A Review and Synthesis of Current Literature.

PBS&J (2007). Rainbow River 2005 Vegetation Mapping and Evaluation Report. Prepared for Southwest Florida Water Managment District. Brooksville, Florida.

Payn, R. A., J. R. Webster, P. J. Mulholland, H. M. Valett, and W. K. Dodds. 2005. Estimation of stream nutrient uptake from nutrient addition experiments. Limnology and Oceanography Methods 3: 174–182.

Quinlan, E. L., Phlips, E. J., Donnelly, K. a., Jett, C. H., Sleszynski, P., & Keller, S. (2008). Primary producers and nutrient loading in Silver Springs, FL, USA. Aquatic Botany, 88, 247–255. http://doi.org/10.1016/j.aquabot.2007.11.003

Reddy, R., & DeLaune, R. (2008). Biogeochemistry of Wetlands. Baca Raton, FL: Taylor and Francis.

Redfield C. 1958. The biological control of chemical factors in the environment. American Scientist 46: 205-221.

Runkel, R. L. 2007. Toward a transport based model of nutrient spiraling and uptake in streams. Limnology Oceanography: Methods 5: 50–62

Sanderson, B. L., Coe, H. J., Tran, C. D., Macneale, K. H., Harstad, D. L., & Goodwin, A. B. (2009). Nutrient limitation of periphyton in Idaho streams: results from nutrient diffusing substrate experiments. Journal of the North American Benthological Society, 28(4), 832–845. http://doi.org/10.1899/09-072.1

Sickman, J. O., Albertin, A., Anderson, M., Pinowska, A., & Stevenson, R. J. (2007). Estimation of autochthonous sources of C, N and P in Florida Springs. Tallahassee, Florida.

Smolders, A. J. P., Hendriks, R. J. J., Campschreur, H. M., & Roelofs, J. G. M. (1997). Nitrate induced iron deficiency chlorosis in Juncus acutiflorus. Plant and Soil, 196(1), 37–45.

Springfield, V. T. (1966). Artesian Water in Teriary Limestone in the Southeastern States. In Geophysical Field Investigations. Department of the Interior.

Stevenson, R., Pinowska, A., Albertin, A. R., & Sickman, J. (2004). Ecological Condition of Algae and Nutrients in Florida Springs. Tallahassee, Florida.

Stream Solute Workshop. 1990. Concepts and methods for assessing solute dynamics in stream ecosystems. Journal of the North American Benthological Society 9: 95–119

Szafraniec, M. L. (2014). Spectral distribution of light in florida spring ecosystems: factors affecting the quatity and quality of light available for primary producers. University of Florida.

Tank, J. L., & Dodds, W. K. (2003). Nutrient limitation of epilithic and epixylic biofims in ten North American streams. Freshwater Biology, 1031–1049.

Water & Air Research Inc. 2016. Final Report for Rainbow River 2015 Aquatic Vegetation Coverage. Report for the Southwest Florida Water Management District, Brooksville FL.

Water & Air Research, Inc. (1991). Diagnostic Studies of the Rainbow River. Prepared for Southwest Florida Water Management District. Brooksville, Florida.

Water & Air Research, Inc. (2016) Final report for Rainbow River 2015 Aquatic Vegetation Coverage. Prepared for Southwest Florida Water Management District. Brooksville, Florida.

Wetland Solutions Inc. 2010. An Ecosystem--Level Study of Florida's Springs. Florida Fish and Wildlife Conservation Commission Project No. 08010

Xiao, K., Yu, D., & Wu, Z. (2007). Differential effects of water depth and sediment type on clonal growth of the submersed macrophyte Vallisneria natans. Hydrobiologia, 589(1), 265–272. http://doi.org/10.1007/s10750-007-0740-4

Zimba, P., M. S. Hopson and D. E. Colle. 1993. Elemental composition of five submersed aquatic plants collected from Lake Okeechobee, Florida. Journal of Aquatic Plant Management 31: 137-140.